

# Reply to reviewers

January 17, 2020

We would like to thank the two reviewers for their detailed feedback and suggestions to improve the article. In the next sections, the reviewers comments are copied and answered per comment (blue color). An additional document is provided that highlights all modifications with respect to the initial submitted version.

## Reviewer 1 (Javier Sanz Rodrigo)

### General Assessment

Interesting paper extending the range of idealized ABL models to include more realistic scaling in unstable conditions in connection to wind energy design tools. I appreciate the effort of the authors in explaining the derivation of the extended model from original models dating back to Ekman (1905). This, in itself, makes the paper worthy of publication to understand a historical perspective on ABL modeling. The authors convincingly demonstrate the scaling properties of the ABL limited-mixing-length model when using Rossby-based length scales which is convenient to reduce the dimensionality of ABL parameterization. The model has a good theoretical basis to provide a more realistic framework for design tools than traditional surface-layer models while it still struggles at reproducing real ABL profiles that are inherently transient and driven by non-uniform forcing. This is demonstrated with a series of validation cases.

There is some clarification to be made on the use or not of local-scaling in stable conditions and, in general, the use of  $u^*$  vs  $G$  and how this could affect Rossby similarity. This is discussed in page 13 but maybe I should be motivated before the model derivation.

In the conclusions, I miss a more extended discussion about the applicability of this model for wind energy applications and challenges that will arise when dealing, for instance, with complex terrain or wake effects. Will the same length scales apply? Will there be additional length scales?

### Major Remarks

1. In the derivation of the model, we end up having three Rossby numbers related to  $z_0$ ,  $l_{\max}$  (or  $l_{\text{ABL}}$  in stable conditions) and  $L$  length scales. All three use  $G/\text{abs}(fc)$  to come up with the non-dimensional number. I understand the convenience of using the same velocity scale for all three parameters but somehow it implies that there is global scaling for all stability conditions. Since we know that the stable ABL depends on local scaling (e.g. Nieuwstadt, JAS-14, 1984) through  $z/L$  I would like to confirm if this is already implicit in  $l_{\max}$  through equation (13). If so, I would suggest that  $L$  is defined as the local Obukhov length when it is first introduced in equation (11). Otherwise, if  $L$  is the surface Obukhov length (as suggested in page 10-21) then you could expect some difficulties of the model to fit very stable profiles as it might be the case in Figure 8.

It's nice to consider very stable cases and local similarity. Recall that MOST is a surface-layer theory in stable conditions, for common values of  $1/L$ ; local scaling arises at larger values of  $z/L$  (see e.g. Wyngaard, 2010 text). We use the original definition of  $L$  (nonlocal); this is consistent with the modelling, which includes  $L$  prescribed via  $\phi$ -functions—which are ASL-based. The very stable case in Fig. 8 has  $z/L < 1$  ( $L^{-1} = 0.036 \text{ m}^{-1}$ ), not in the range of local-similarity (valid for  $z/L \gg 1$ ; local

MOST can arise in the RANS equations, if buoyancy is implemented differently, e.g. via  $d\theta/dt$  equation and source terms in  $\{w, k, \varepsilon\}$ .)

2. Along this local-scaling reasoning, I would find it more appropriate to use  $u^*$  as a velocity scale in relation to  $l_{ABL}$  which depends on  $z/L$ , with  $L$  being a local quantity. Actually, you can generalize  $l_{ABL}$  to unstable conditions by simply using the equivalent Dyer functional forms of the stability function  $\phi_m(z/L)$ . In this alternative formulation you would have  $z_0$ ,  $l_{max}$  (Blackadar) and  $L$  as length scales with  $z_0$  and  $l_{max}$  being global scales and  $L$  being local scale. I'm not sure if this would work out in terms of Rossby similarity, as you mention at the beginning of page 13.

This is a good point. We (the authors) had discussions about the use of either  $G$  versus  $u_{*0}$ , and purposefully decided to use  $G$ . It is more convenient to use  $G$  instead of  $u_{*0}$ , because  $G$  is a model input, while  $u_{*0}$  is a model result. In addition,  $u_{*0}$  in practice can become a function of height (more so for shallower ABLs, despite being assumed constant); i.e., the height at which  $u_{*0}$  is diagnosed then becomes an extra 'input'. However, it is possible to obtain a Rossby similarity based on ideal (constant, ASL value)  $u_{*0}$ . We have now added an Appendix (Appendix B) showing exactly this, which makes the Rossby similarity more general—since the choice of velocity scale does not affect the similarity. We have also defined three alternative Rossby numbers based on  $u_{*0}$ , which can be written in terms of the Rossby numbers based on  $G$  and the geostrophic drag coefficient  $u_{*0}/G$ :

$$\text{Ro}_\ell^* \equiv \frac{u_{*0}}{|f_c| \ell_{\max}} = \frac{u_{*0}}{G} \text{Ro}_\ell, \quad \text{Ro}_0^* \equiv \frac{u_{*0}}{|f_c| z_0} = \frac{u_{*0}}{G} \text{Ro}_0, \quad \text{Ro}_{L-}^* \equiv \frac{-u_{*0}}{|f_c| L} = \frac{u_{*0}}{G} \text{Ro}_{L-}$$

The geostrophic drag coefficient  $u_{*0}/G$  as plotted in Fig. 6 can thus be transformed as an explicit relation of  $\text{Ro}^*$ ,  $\text{Ro}_0^*$  and  $\text{Ro}_{L-}^*$ . This information gives the value  $G$  needed to obtain a desired  $u_{*0}$  for Rossby numbers based on  $u_{*0}$ . Figure 1 below depicts the Rossby similarity based on  $u_{*0}$  using the limited length scale  $k$ - $\varepsilon$  model for neutral conditions ( $\text{Ro}_{L-}^* = 0$ ); but we note it also works for  $\text{Ro}_{L-}^* \neq 0$  and using the limited mixing-length model instead of the limited length scale  $k$ - $\varepsilon$  model.

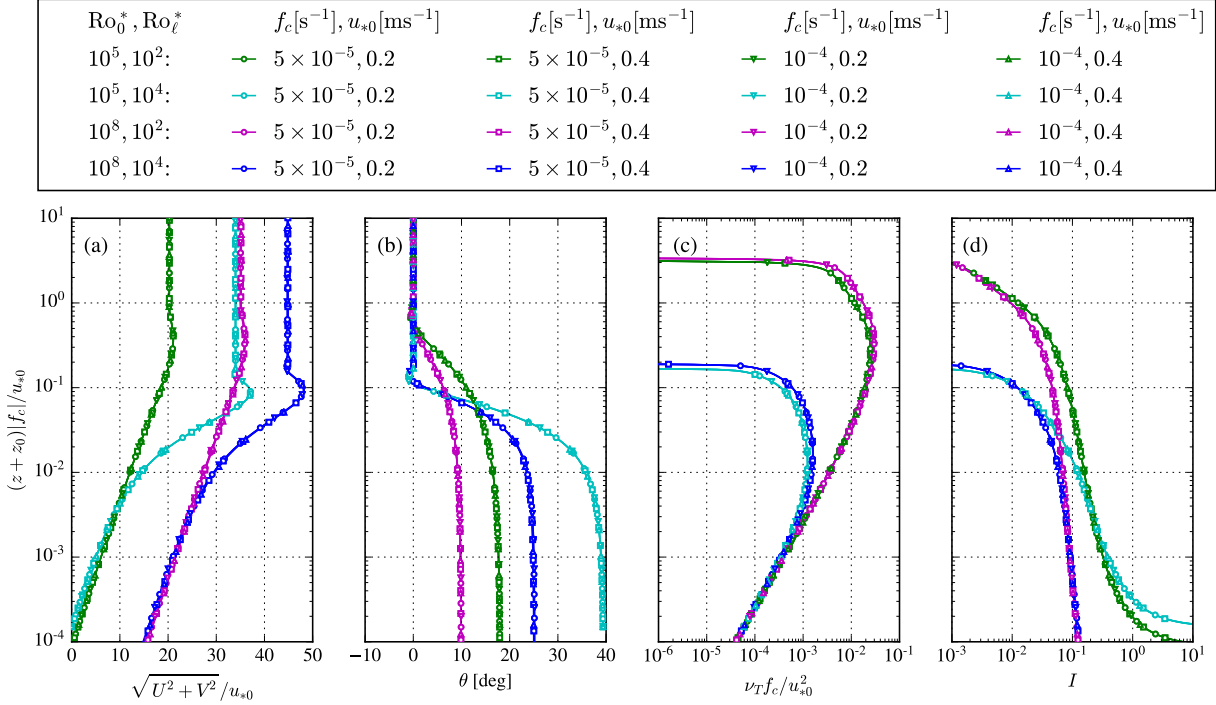


Figure 1: [In response to major remark #2] Rossby number similarity of the limited length scale  $k$ - $\epsilon$  model using the friction velocity as the velocity scale, for neutral conditions ( $Ro_{L-} = 0$ .)

Regarding use of the unstable  $\phi_m$  function to extend  $\ell_{\max}$  for unstable conditions, this is exactly what we do for the mixing-length model, where the turbulence length scale is prescribed analytically (see Section 3.1 and Eqns. 9-11). This does not work for the limited length scale  $k$ - $\epsilon$  model of Apsley and Castro, because the turbulence length scale is always smaller than  $\kappa z$ , no matter what the value of  $\ell_{\max}$  is (except for a possible overshoot near the ABL height). To include length scales that are larger than  $\kappa z$ , one needs to include an additional model behavior, i.e. buoyancy source terms in the turbulence transport equations as given in Section 3.2.

We remind that local scaling is not valid for unstable conditions (though mixed-layer scaling arises in the unstable ABL), again consistent with our  $L$  being surface-based.

- Page 6, Equation (13): I would define  $l_{ABL} = l_{\max}$  for  $z/L = 0$  and  $l_{ABL} = [1/l_{\max} + \beta/(\kappa L)]^{-1}$  and use  $l_{ABL}$  in the definition of  $Ro_l$  (21) since  $l_{\max}$  is originally associated with Blackadar's mixing length for neutral conditions and you will use  $Ro_l$  for both neutral and stable conditions. Then, equation (21) would be based on  $l_{ABL}$ , and not  $l_{\max}$  right?

We understand that one could parametrize the (stable) turbulence length scale of the ABL,  $\ell_{ABL}$ , using a stable  $\phi_m$  function, as shown by Apsley and Castro (1997). However, one could also think of a more general  $\ell_{ABL}$  by not only using  $\ell_{\max}$  and  $\phi_m$ , but also including additional length scales that could influence  $\ell_{ABL}$ , e.g., entrainment. This is something we plan to look at in future work. In addition, your second (stable) definition of  $\ell_{ABL}$ , can be rewritten as an effective  $\ell_{\max}$ , as shown in Eq. (13), hence a stable  $L$  is not an independent parameter and therefore, we use a Rossby number based on  $\ell_{ABL} = \ell_{\max}$ . This is not the case for unstable conditions, where the  $\phi_m$  function is not linear in  $z/L$ , and therefore we end up with third independent parameter in form of an unstable  $L$  or its associated Rossby number. We have added a small clarification about the effective  $\ell_{\max}$  at the end of Section 3.1 as a response to the second reviewer.

## Minor Remarks

1. Page 1-15: “Such a model should be simple enough to be applicable in the wind energy industry” It sounds a bit like industry could not handle complex models. Maybe, “... to be efficiently used in design tools”.  
You are right, this sentence can be interpreted in that way. We mean that the wind energy industry can benefit more from simple and fast models that are often more easy to be adapted in a chain of design tools compared to high fidelity models. We have changed the sentence to: *Such a model should be simple enough to efficiently improve the chain of design tools used by the wind energy industry.*
2. For completeness, I think you should mention in the introduction other hypothesis that apply to the model even if some of them are mentioned in the derivation later on: dry-atmosphere, no mesoscale advection, no vertical wind speed, etc.  
We have added *here we exclude effects of flow inhomogeneity and nonstationarity, which are typically considered by mesoscale and three-dimensional time-varying model in: Idealized, steady-state models can represent long-term averaged velocity and turbulence profiles of the real ABL, including the effects of Coriolis, atmospheric stability, capping inversion, homogeneous surface roughness and flat terrain; here we exclude effects of flow inhomogeneity and nonstationarity, which are typically considered by mesoscale and three-dimensional time-varying models.* We think that all the other assumptions are stated clear enough in the introduction.
3. 2-16: Even if you mention them later, please provide references to the “Blackadar-type” models to provide a more meaningful introduction of the type of models that you try to improve from.  
We now refer to Blackadar (1962). In addition, we have rephrased a sentence in Section 3.2 to: *In stable conditions,  $\phi_m = 1 + \beta z/L$ , so the resulting turbulence length can also be rewritten in the form of Eqs. (4) and (9),...*
4. 5-18: Consider changing the title of the section to “Limited mixing-length model in stable conditions” since the objective is to define `L_ABL` which, in this formulation, do not include unstable conditions  
In this Section, we start with the original models, suited for stable and neutral conditions, and then extend it to unstable conditions. Hence adding “for stable conditions” to the subsection title does not make sense. We have decided to keep the current title.
5. 7-9: For clarity, “... all have the same coefficient: `C_epsilon,2`.”  
Adapted.
6. 8-12: A rough-wall boundary condition  
Corrected.
7. 9-7: `L` was used before to denote the Obukhov length. Although I think it is clear from the context, I would rather use `U*` and `L*` or anything else to denote that these are generic velocity and length scales, not to be confused with `U` and `L` elsewhere in the paper.  
This is a good point. We have now used  $\mathcal{U}$  and  $\mathcal{L}$  as the characteristic velocity and length scales.
8. 9-10: “`Ro_l` is analogous to the reciprocal of a dimensionless boundary layer depth” Maybe you could add the dimensionless boundary layer depth for clarity. This will help when you interpret equation (23) as a ratio of `z_i/z_0` (page 10-1)  
We have added  $z_i f_c / u_{*0}$ .
9. Equation (22): Following previous comment, you may consider naming `l_b = G/abs(fc)` as a “master” length scale (not sure about the most appropriate name) since this is present throughout the paper and you also use this to plot non-dimensional height in Figures that follow.  
Such a master length scale could be used, but we prefer to stick with  $G$  and  $f_c$  in the plots because they are well-known quantities.
10. 16-9: Why the blue line and not the yellow line with  $A = 2$  and  $B = 4.42$  being somehow closer to  $A = 1.8$  and  $B = 4.5$  (Troen and Petersen)?  
The simple ‘blue’ statement arose from an earlier version of the plot. We now correct; *For moderate*

*roughness lengths over land, the measured values tabulated by Hess and Garratt (2002) generally fall between the blue and yellow lines for neutral conditions, which are consistent with the typically used values in wind energy are  $A = 1.8$  and  $B = 4.5$  (e.g. Troen and Petersen, 1989).*

## Reviewer 2 (Anonymous)

In this paper, a one-dimensional RANS model is used to simulate idealised ABL profiles and shows that, for neutral and stable conditions, the Blackadar limited length scale model, and the limited length-scale k-e model of Apsley and Castro produce profiles that can be described by two Rossby numbers: one using  $z_0$  as the characteristic lengthscale, the other one using the maximum turbulence lengthscale defining the model. For unstable conditions, an extension is proposed to the limited lengthscale k-e model, which produce profiles characterised by a third Rossby number depending on the Obukhov lengthscale. The model derived drag law parameters  $A$   $B$  fit well within the range of observed typical  $A$   $B$  values. The model's ability to reproduce measured ABL profiles is tested with a varying level of success. The investigation is interesting, and potentially useful to provide inflow boundary conditions to a 3D model from a library of precalculated profiles. The application of the derived profiles within a 3D model hasn't been attempted yet in this contribution. The paper is generally well written, although some points/comments should be addressed as listed below.

### Specific comments:

1. p.1, line 16. What does 'simple enough to be applicable in the wind energy industry' mean? So it can be used for wind turbine design? So it can be used as inflow b.c. for a flow model?

*We mean that the wind energy industry can benefit more from simple and fast models that are often more easy to be adapted in a chain of design tools compared to high fidelity models. We have changed the sentence to: *Such a model should be simple enough to efficiently improve the chain of design tools used by the wind energy industry.**

2. P.1, line 24-25. 'These turbulence models can simulate stable and neutral ABLs without the necessity of a temperature equation and a momentum source term of buoyancy. In other words, all temperature effects are represented by the turbulence model'. This is only true when looking at horizontally homogeneous flows (i.e. the 1D flows modelled in this paper). Once terrain, coastal discontinuities, or even an offshore wind farm is perturbing the flow, gravity waves can develop, which have the potential to affect the wind speed distribution at hub height. And to capture these you need the buoyancy source term in the momentum equation. Please elaborate on these. Your statement as it is can be misleading and let the reader assume that they can generally ignore the buoyancy in the momentum equation.

*This is a valid point. One may need a buoyancy source term in the momentum equation to accurately model the effects of stability in complex terrain and wind farms. However, we don't know how much the simplification (of modeling the effect of stability without a momentum source term of buoyancy) would affect the flow. We have added **one dimensional** in the introduction: *These turbulence models can simulate one dimensional stable and neutral ABLs without the necessity of a temperature equation and a momentum source term of buoyancy.* In addition, we have added a small discussion on this topic at the end of the conclusion: *In addition, the effects of length scale limitation and neglecting the buoyancy force in the momentum equation need to be quantified for three-dimensional RANS simulations of complex terrain and wind farms.**

3. p.6 equation 13. We have two  $l_{max}$  here,  $l_{max}$  and  $l_{max,eff}$ . Am I right in understanding that when later on there is a reference to  $l_{max}$  it is in fact  $l_{max,eff}$ ? i.e. the Rossby number as a function of  $l_{max}$  or the fitted values of  $l_{max}$  in Table 2 are referring to values of  $l_{max,eff}$ ? Is eq 13 used at all in your model? Probably worth clarifying... especially if I have misunderstood.

*Equation (13) is just to show that it does not make sense to define a surface layer turbulence length scale,  $\ell_{ASL}$ , based on MOST for stable conditions, because one would obtain the original turbulence length scale expression of Blackadar (1962). We have added clarifying text: *Thus we can simply use the original length scale model of Blackadar (1962) for stable and neutral conditions; the stable  $\phi_m$  function simply informs the selection of  $\ell_{max,eff}$ , following Eq. (13).**

4. p.6. extended turbulence model for unstable flows: am I right in understanding that the buoyancy term  $B$  added to the k-e equations is only added for unstable flows. i.e. when you model neutral or stable cases listed in Table 2, you only use the original length scale limited model of Apsley and Castro?

That is correct. One could add the buoyancy terms for neutral conditions, but they would be zero because then we have  $1/L = 0$ .

5. p.8. Numerical set up. How is convergence defined? I'm trying to understand how the overall momentum balance is achieved. We have friction at the ground, so a momentum sink, no wind speed gradient at the top (so no shear driven flow). As friction is reduced or increased I'd expect the boundary layer height to reduce or grow vs time. Do you judge convergence based on the boundary layer growth? Do you prescribe a pressure gradient in the flow direction? Worth elaborating?

The flow is driven by a set geostrophic wind speed  $G$ , which represents a constant prescribed pressure gradient, i.e.  $\partial P/\partial x = \rho f_c V_G$  and  $\partial P/\partial y = -\rho f_c U_G$ . A balance between the pressure gradient, Coriolis force and the turbulence generated from the ground is achieved when the convergence has been achieved. The convergence is defined as the equation residual normalized by the initial guess, which is a uniform flow with the  $G$  as the wind speed. We have added to Section 4.2: *The flow is driven by a constant pressure gradient using a prescribed constant geostrophic wind speed. The initial wind speed is set to the geostrophic wind speed. During the solving procedure the ABL depth grows from the ground until convergence is achieved, which occurs when the growth of the ABL depth is negligible because a balance of the prescribed pressure gradient, Coriolis forces and turbulence stresses is obtained.*

6. p.8. Numerical set up. Boundary condition at the ground: is it using the neutral formulation even when modelling stable or unstable cases? Did you try changing the closure at the wall using stability dependent closures?

We use the same rough wall boundary conditions in neutral and non-neutral conditions. This is because the flow near the wall is following a neutral logarithmic profile, also in non-neutral conditions. Our first cell height is small enough (0.1 m) to be in this region and we do not need to extend the boundary conditions for non-neutral conditions. One could also see from the wind speed profile based on MOST, that one obtains the neutral logarithmic profile near the wall since  $z/L \rightarrow 0$ .

7. p.9. line 4. I find the sentence 'We find that if both  $l_{max}$  and  $z_0$  are proportional to ...' a bit of a back to front way to introduce Rossby number similarity. My first reaction when reading this was that  $z_0$  is usually an input parameter that depends on the ground conditions, therefore why should it be proportional to  $G/f_c$ . Worth rewriting?

We understand that this is somewhat confusing. We have now rewritten the first part of Section 5, where we have added a full derivation of the three Rossby numbers by introducing normalized variables in the momentum equation.

8. P9. Line 6. The general definition of  $Ro$  as a function of  $U$  and  $L$  where  $U$  and  $L$  are characteristic wind speed and velocity scales is fine on its own. But in the current context, where the symbol  $L$  has also been used for the Obukhov length, the use of  $L$  for a general lengthscale is a bit unfortunate. Especially since you proceed using  $L$ , the Obukhov length, when later defining  $RO\_L$ . I would suggest using a different symbol for  $L$  here, may be using a different font.

This is a good point. We now used  $\mathcal{U}$  and  $\mathcal{L}$ .

9. p.14, equation 25. I know it's common to use the  $A$  and  $B$  notation for the 'constants' in the GDL, but it's unfortunate that  $B$  was also the symbol used for the buoyancy term earlier on. I'd suggest avoiding the use of the same symbol for both.

This is also good point. We have changed the Buoyancy variable  $B$  to  $\mathcal{B}$ .

10. p.16, line 8. The fact that the  $A$  and  $B$  parameters in the DGL are function of the stability (via  $l_{max}$  or  $L$ ) is not new. While not necessarily formulated as a function of the Rossby numbers used in the current publication, their dependence on the Obukhov length and on the Brundt Vaysala frequency has been discussed quite a while ago. See e.g. Landberg for dependence in  $\mu$  (i.e. Obukhov length) Landberg, L., 1994, 'Short term prediction of local wind conditions', Risoe National Laboratory, Roskilde,

Denmark or Zilitinkevich (1989) already referred to. This would be worth including in the discussion. We added: *This is not a surprising result, since many authors showed that A and B are dependent on atmospheric stability (see, e.g., Arya 1975; Zilitinkevich 1989; Landberg 1994).*

11. p.18, Figure 8. Plot of the turbulence lengthscale. What is happening with the plot of the very stable case at the top of the ABL? Is the black line really the solution of the 1D CFD?

We obviously forgot to discuss this result. The simulated very stable case has an ABL depth around 100 m, see Fig. 8a. When the gradient  $dU/dz$  is taken around the ABL depth, we get  $dU/dz \rightarrow 0$  so that  $\hat{\ell} = u_{*0}/(dU/dz) \rightarrow \infty$ , which results in a spike in Fig 8b. We have added some clarification in the text: *... and the model predicts an ABL depth of about 100 m, which results in a spike in  $\hat{\ell}$ , since  $dU/dz$  is zero around the ABL depth.*

12. p.21. I find the discussion somewhat lacking on the fact that the profiles obtained by fitting both G, lmax were well captured, while those where only lmax was varied were not so well captured. Could it be because the role of lmax is to reflect the ABL height, while at the same time be accounting for surface stability effects? Should there be a third lengthscale also entering the definition of the stable profiles so that the role of limiting effects at the surface (via L) and limiting effects at the top of the boundary layer (via the Brunt Vaysala frequency) can be treated independently? This might provide the additional degree of freedom that the model seems to require to fit the measured profiles. (degree of freedom which was provided by allowing the model to fit G). This sort of dependency was proposed by Zilitinkevich and Mironov (1996) and it's use suggested in Zilitinkevich et al (1996). Worth discussing? Zilitinkevich S.S., Mironov, D.V., 1996, 'A Multi-Limit Formulation For The Equilibrium Depth Of A Stably Stratified Boundary Layer', Bound. Layer Meteorol., 81, pp 325-351. Zilitinkevich S.S., Johansson P.-E., Mironov D.V., Baklanov A., in press, 'An Analytical Similarity Theory Model For Wind Profile And Resistance Law In Stably Stratified Planetary Boundary Layers', J. Wind. Eng. Industr. Aerodyn, 74-76 (1998) 209-218.

This is an interesting point, which we had discussed in previous months; we have plans to extend the  $k-\epsilon$  model further to include effects of an inversion strength (via e.g.  $N_{BV}$ ), as this is very important parameter for wind farm simulations subjected to atmospheric inflow. However, we chose and prefer to save this discussion for an upcoming article, because we would need to add a significant part, to an already lengthy article.

13. P.21, line 25 '...dependence upon two Rossby numbers, which correspond to the roughness length and the maximum turbulence length scale' should be rewritten. 'correspond' is not exactly appropriate, may be use 'defined from' instead.

Adapted.

14. p.22. The Obukhov length is dimensional, while the Rossby number is not. So the sentence '...the Obukhov length, which can also be written as a third Rossby number' should be changed. Likely something along the lines of 'The Obukhov length can be used to define a third Rossby number'.

Adapted.

15. p.22. The conclusion feels like it was hastily written. When I first read the abstract, introduction and conclusion, I could not quite understand what various parts of the conclusion referred to. I feel the conclusions should be improved, so that they can provide a clearer summary of what was done, so they can stand on their own without having to read through the whole article. For example, the content of the sentence 'A model validation of the full ABL for a stable, a neutral and an unstable case is performed, with less success for the non-neutral cases.' could be explained a bit more. i.e. what is meant by a full validation? Also, the results of the validation could be detailed a bit more than the rather succinct 'with less success for the non-neutral case'.

In general we like a short conclusion, but we understand that we could improve it based on your suggestions. We have remove the word *full* from *full ABL* because we just mean a boundary layer profile that does not only corresponds to a surface layer. In addition, we have added *In the very stable case, the measured wind veer of 50° was larger than the maximum wind veer of 45° that the k-ε model can simulate. In addition, the very unstable case was characterized by non-stationary conditions, which are difficult to capture with a RANS model.*

### Technical corrections:

1. p.2, line 31. Negative sign missing in front of  $u'w'$  and  $v'w'$ .  
Corrected.
2. p.2 eq (1). Should be a positive sign in front of the diffusion terms  
Corrected.
3. p.8, line 12. Comma instead of full stop after 'at the ground'  
Corrected.
4. p.14, line 6. Should be proportional to minus a  $\log_{10}(Ro-1)$  (negative slope in Fig 5)  
Corrected.
5. p.24. Zilitinkevich reference is missing the journal.  
Corrected.

# Rossby number similarity of atmospheric RANS using limited length scale turbulence closures extended to unstable stratification

Maarten Paul van der Laan<sup>1</sup>, Mark Kelly<sup>1</sup>, Rogier Floors<sup>1</sup>, and Alfredo Peña<sup>1</sup>

<sup>1</sup>Technical University of Denmark, DTU Wind Energy, Risø Campus, Frederiksborgvej 399, 4000 Roskilde, Denmark

**Correspondence:** Maarten Paul van der Laan (plaa@dtu.dk)

**Abstract.** The design of wind turbines and wind farms can be improved by increasing the accuracy of the inflow models representing the atmospheric boundary layer. In this work we employ one-dimensional Reynolds-averaged Navier-Stokes (RANS) simulations of the idealized atmospheric boundary layer (ABL), using turbulence closures with a length scale limiter. These models can represent the mean effects of surface roughness, Coriolis force, limited ABL depth, and neutral and stable atmospheric conditions using four input parameters: the roughness length, the Coriolis parameter, a maximum turbulence length, and the geostrophic wind speed. We find a new model-based Rossby similarity, which reduces the four input parameters to two Rossby numbers with different length scales. In addition, we extend the limited length scale turbulence models to treat the mean effect of unstable stratification in steady-state simulations. The original and extended turbulence models are compared with historical measurements of meteorological quantities and profiles of the atmospheric boundary layer for different atmospheric stabilities.

## 1 Introduction

Wind turbines operate in the turbulent atmospheric boundary layer (ABL) but are designed with simplified inflow conditions that represent analytic wind profiles of the atmospheric surface layer (ASL). The ASL corresponds to roughly the first 10% of ABL, typically less than 100 m, while the tip height of modern wind turbines are now sometimes beyond 200 m. Hence, there is a need for inflow models that represent the entire ABL in order to improve the design of wind turbines and wind farms. Such a model should be simple enough to ~~be applicable in~~ efficiently improve the chain of design tools used by the wind energy industry.

The ABL is complex and changes continuously over time. Idealized, steady-state models can represent long-term averaged velocity and turbulence profiles of the real ABL, including the effects of Coriolis, atmospheric stability, capping inversion, ~~a~~ homogeneous surface roughness and flat terrain; here we exclude effects of flow inhomogeneity and nonstationarity, which are typically considered by mesoscale and three-dimensional time-varying models. In this work, we investigate idealized ABL models that are based on one-dimensional Reynolds-averaged Navier-Stokes (RANS), where the only spatial dimension is the height above ground. The output of the model can be used as inflow conditions for three-dimensional RANS simulations of complex terrain (Koblitz et al., 2015) and wind farms (van der Laan and Sørensen, 2017b). Turbulence is here modeled by two limited length scale turbulence closures, the mixing-length model of Blackadar (1962) and the two equation  $k$ - $\varepsilon$  model

of Apsley and Castro (1997). These turbulence models can simulate [one dimensional](#) stable and neutral ABLs without the necessity of a temperature equation and a momentum source term of buoyancy. In other words, all temperature effects are represented by the turbulence model. The limited length scale turbulence models depend on four parameters: the roughness length, the Coriolis parameter, the geostrophic wind speed and a chosen maximum turbulence length scale that is related to the ABL depth. We show that the normalized profiles of wind speed, wind direction and turbulence quantities are only dependent on two dimensionless parameters that represent the ratio of the inertial to the Coriolis force, based on two different length scales; the roughness length and the maximum turbulence length scale. These dimensionless parameters are Rossby numbers. The Rossby number based on the roughness length is known as the surface Rossby number as introduced by Lettau (1959), while the Rossby number based on the maximum turbulence length is a new dimensionless parameter. The obtained model-based Rossby number similarity is used to validate a range of simulations with historical measurements of geostrophic drag coefficient and cross isobar angle. In addition, we show that both RANS models' solutions are bounded by two analytic solutions of the idealized ABL.

The limited length scale turbulence closures of Blackadar (1962) and Apsley and Castro (1997) can model the effect of stable and neutral stability but cannot model the unstable atmosphere. We propose simple extensions to solve this issue and validate the results of the extended  $k-\varepsilon$  model with measurements of wind speed and wind direction profiles. The model extensions lead to a third Rossby number, where the length scale is based on the Obukhov length. The limited mixing-length model is not considered in the comparison with measurements because we are mainly interested in the limited length scale  $k-\varepsilon$  model. The  $k-\varepsilon$  model is more applicable to wind energy applications because it can also provide an estimate of the turbulence intensity, which is not available from [the limited mixing-length \(Blackadar type\) models](#) [model of Blackadar \(1962\)](#). The limited mixing-length model is applied here to show that the same model-based Rossby number similarity is recovered as obtained for the  $k-\varepsilon$  model.

The article is structured as follows. Background and theory of the idealized ABL are discussed in Section 2. Extensions to unstable surface layer stratification are presented in Section 3. Section 4 presents the methodology of the one dimensional RANS simulations. The model-based Rossby similarity is illustrated in Section 5. The simulation results of the limited length scale  $k-\varepsilon$  model including the extension to unstable conditions are compared with measurements in Section 6.

## 2 Background and theory: idealized models of the ABL

We model the mean steady-state flow in an idealized ABL. Here idealized refers to flow over homogeneous and flat terrain under barotropic conditions such that the geostrophic wind does not vary with height. This flow can be described by the incompressible RANS equations for momentum, where the contribution from the molecular viscosity is neglected due to the high Reynolds number:

$$\frac{DU}{Dt} = f_c(V - V_G) - \frac{d}{dz} \left( \nu_T \frac{dU}{dz} \right) = 0, \quad \frac{DV}{Dt} = -f_c(U - U_G) - \frac{d}{dz} \left( \nu_T \frac{dV}{dz} \right) = 0, \quad (1)$$

where  $U$  and  $V$  are the mean horizontal velocity components,  $U_G$  and  $V_G$  are the corresponding mean geostrophic velocities,  $f_c = 2\Omega \sin(\lambda)$  is the Coriolis parameter with  $\Omega$  as Earth's angular velocity and  $\lambda$  as the latitude, and  $z$  is the height above

ground. In addition, the Reynolds-stresses  $\overline{u'w'}$  and  $\overline{v'w'}$  are modeled by the linear stress-strain relationship of Boussinesq (1897):  $\overline{u'w'} = \nu_T dU/dz$  and  $\overline{v'w'} = \nu_T dV/dz$ , where  $\nu_T$  is the eddy viscosity. The boundary conditions for  $U$  and  $V$  are:  $U = V = 0$  at  $z = z_0$  and  $U = U_G$  and  $V = V_G$  at  $z \rightarrow \infty$ , where  $z_0$  is the roughness length. Note that it is possible to write the two momentum equations as a single ordinary differential equation:

$$5 \quad \frac{d}{dz} \left( \nu_T \frac{dW}{dz} \right) = i f_c W, \quad (2)$$

where  $W \equiv (U - U_G) + i(V - V_G)$  is a complex variable and  $i^2 = -1$ .

The eddy viscosity,  $\nu_T$ , needs to be modeled in order to close the system of equations. The eddy viscosity can be written as  $\nu_T = u_* \ell$ , where  $u_*$  and  $\ell$  represent turbulence velocity and turbulence length scales. For a constant eddy viscosity, the equations can be solved analytically and the solution is known as the Ekman spiral (Ekman, 1905), which includes the wind direction change with height due to Coriolis effects. The Ekman spiral can also be considered a laminar solution, since one can neglect the turbulence in the momentum equations and set the molecular viscosity to determine the rate of mixing. For an eddy viscosity that increases linearly with height, the equations can also be solved analytically, as introduced by Ellison (1956) and discussed by Krishna (1980) and Constantin and Johnson (2019). The two analytic solutions are provided in Appendix A. One can relate the analytic solution of Ellison (1956) to the (neutral) ASL ( $z \ll z_i$ ), while the Ekman spiral is more valid for altitudes around the ABL depth  $z_i$ . Neither of the two analytic solutions result in a realistic representation of the entire (idealized) ABL. A combination of both a linear eddy viscosity for  $z \ll z_i$  and a constant eddy viscosity for  $z \sim z_i$  should provide a more realistic solution. For example, the eddy viscosity could have the form  $\nu_T = \kappa u_{*0} z \exp(-z/h)$ , where  $\nu_T$  increases linearly with height for  $z \ll h$  as expected in the surface layer, then it reaches a maximum value at  $z = h$ , and decreases to zero for  $z > h$ . Note that  $u_{*0}$  is the friction velocity near the surface. Constantin and Johnson (2019) derived a number of solutions for a variable eddy viscosity, although an explicit solution for the entire idealized ABL with a realistic eddy viscosity (in the previously mentioned form) has not been found yet. Hence, numerical methods are still necessary, and one of the simplest numerical model for the idealized ABL is given by Blackadar (1962) using Prandtl's mixing-length model:

$$\nu_T = \ell^2 \mathcal{S} \quad (3)$$

where  $\mathcal{S} = \sqrt{(dU/dz)^2 + (dV/dz)^2} = |dW/dz|$  is the magnitude of the strain-rate tensor, and prescribed  $\ell$  as a turbulence length scale

$$\ell = \frac{\kappa z}{1 + \frac{\kappa z}{\ell_{\max}}}, \quad (4)$$

where  $\kappa z$  is the turbulence length scale in the neutral surface layer with  $\kappa$  as the von Kármán constant, and  $\ell_{\max}$  is a maximum turbulence length scale. It is also possible to model the eddy viscosity with a two-equation turbulence closure, e.g., the  $k$ - $\varepsilon$  model:

$$30 \quad \nu_T = C_\mu \frac{k^2}{\varepsilon} \quad (5)$$

with  $C_\mu$  as a model parameter,  $k$  as the turbulent kinetic energy and  $\varepsilon$  as the dissipation of  $k$ . Both  $k$  and  $\varepsilon$  are modeled by a transport equation:

$$\frac{Dk}{Dt} = \frac{d}{dz} \left( \frac{\nu_T}{\sigma_k} \frac{dk}{dz} \right) + \mathcal{P} - \varepsilon, \quad (6)$$

$$\frac{D\varepsilon}{Dt} = \frac{d}{dz} \left( \frac{\nu_T}{\sigma_\varepsilon} \frac{d\varepsilon}{dz} \right) + (C_{\varepsilon,1}\mathcal{P} - C_{\varepsilon,2}\varepsilon) \frac{\varepsilon}{k}, \quad (7)$$

5 where  $\mathcal{P}$  is the turbulence production, and  $\sigma_k$ ,  $\sigma_\varepsilon$ ,  $C_{\varepsilon,1}$  and  $C_{\varepsilon,2}$  are model constants that should follow the relationship  $\kappa^2 = \sigma_\varepsilon \sqrt{C_\mu} (C_{\varepsilon,2} - C_{\varepsilon,1})$ . When using the standard  $k$ - $\varepsilon$  model calibrated for atmospheric flows (Richards and Hoxey, 1993), the turbulence length scale or eddy-viscosity will keep increasing until a boundary layer depth is formed and the analytic solution of Ellison (1956) is approximated. Apsley and Castro (1997) proposed to modify the transport equation of  $\varepsilon$ , such that a maximum turbulence length scale is enforced by replacing the constant  $C_{\varepsilon,1}$  with a variable parameter  $C_{\varepsilon,1}^*$ :

$$10 \quad C_{\varepsilon,1}^* = C_{\varepsilon,1} + (C_{\varepsilon,2} - C_{\varepsilon,1}) \frac{\ell}{\ell_{\max}}, \quad (8)$$

where the turbulence length scale is modeled as  $\ell = C_\mu^{3/4} k^{3/2} / \varepsilon$ . This limited-length scale  $k$ - $\varepsilon$  model behaves very similar to the mixing-length model of Blackadar (1962) (Eqs. 3 and 4). For  $\ell \ll \ell_{\max}$ , the surface layer solution is obtained, while for  $\ell \sim \ell_{\max}$ , the source terms in the transport equation of  $\varepsilon$  cancel ( $C_{\varepsilon,1}^* \mathcal{P} \sim C_{\varepsilon,1} \varepsilon$ ), and the turbulence length scale is limited. For a given  $z_0$ ,  $G$ , and  $f_c$ , the ABL depth can be controlled by  $\ell_{\max}$ . This means that  $\ell_{\max}$  is related to  $z_i$ ; Apsley and Castro

15 (1997) noted that  $\ell_{\max} \sim z_i/3$  for typical neutral ABLs. However, the simulated boundary layer depth using the  $k$ - $\varepsilon$  model of Apsley and Castro (1997) has an approximate dependence of  $z_i \propto (G/|f_c|)^{1-a} \ell_{\max}^a$  with  $a \approx 0.6$ , which we will further discuss in Section 5. A summary of the discussed eddy viscosity closures is listed in Table 1. Figure 1 compares the analytic solutions of Ekman (1905) and Ellison (1956) with the numerical solutions of the limited mixing-length model of Blackadar (1962) and the limited length scale  $k$ - $\varepsilon$  of Apsley and Castro (1997) in terms of wind speed, wind direction,  $\theta = \arctan(V/U)$ , and eddy

20 viscosity. The Ekman spiral is depicted with two constant eddy viscosities, which only translates the solution vertically. In addition, we have chosen  $f_c = 10^{-4} \text{ s}^{-1}$ ,  $G = 10 \text{ ms}^{-1}$ , and  $z_0 = 10^{-2} \text{ m}$ . The numerical solutions are shown for a range of  $\ell_{\max}$  values. It is clear that the ABL depth decreases for lower values of  $\ell_{\max}$ , for both numerical models, and their solutions behave similarly. A lower  $\ell_{\max}$  also results in a higher shear and wind veer, and a lower eddy viscosity, which are characteristics of a stable ABL. Hence, the limited length scale turbulence closures can model the effects of stable stratification by solely

25 limiting the turbulence length scale, without the need of a temperature equation or buoyancy source terms. When  $\ell_{\max} \rightarrow 0 \text{ m}$  (note that there is minimal limit of  $\ell_{\max}$  in order to obtain numerically stable results), the solution approaches to the Ekman spiral because the eddy viscosity in the ABL can be approximated by a constant eddy viscosity. Hence, the maximum change in wind direction simulated by the  $k$ - $\varepsilon$  model of Apsley and Castro (1997) is that of the Ekman spiral:  $45^\circ$ . For large  $\ell_{\max}$  values, the numerical solution approximates the analytic solution of Ellison (1956) but does not match it because their eddy

30 viscosities are different for  $z \geq z_i$ .

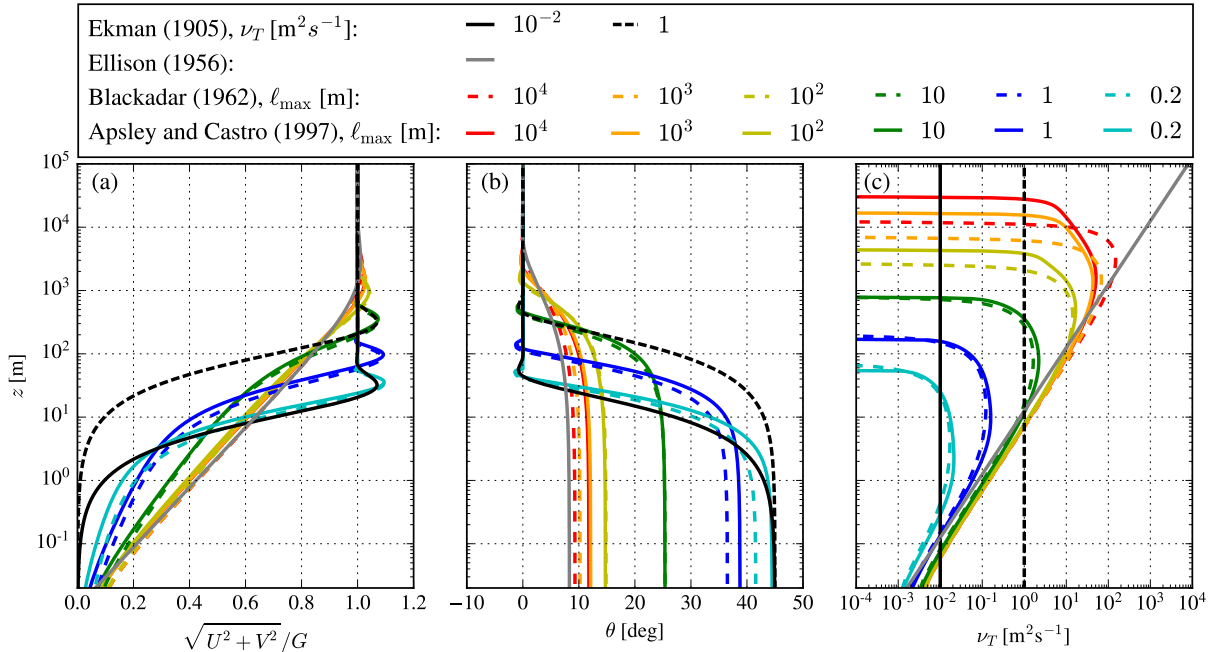


**Figure 1.** Comparison of analytic and numerical solutions of existing idealized ABL models using  $f_c = 10^{-4} \text{ s}^{-1}$ ,  $G = 10 \text{ m s}^{-1}$  and  $z_0 = 10^{-2} \text{ m}$  for different model parameters. **(a)** Wind speed. **(b)** Wind direction. **(c)** Eddy viscosity.

Eddy viscosity closure			Solution	Reference
Constant	-	-	Analytic	Ekman (1905)
Linear	$\nu_T = u_* \ell$	$\ell = \kappa z$	Analytic	Ellison (1956)
Limited mixing-length model	$\nu_T = \ell^2 \mathcal{S}$	$\ell = \kappa z / (1 + \kappa z / \ell_{\max})$ ,	Numerical	Blackadar (1962)
Limited length scale $k$ - $\varepsilon$ model	$\nu_T = C_\mu k^2 / \varepsilon$	$\ell = C_\mu^{3/4} k^{3/2} / \varepsilon$	Numerical	Apsley and Castro (1997)

**Table 1.** Eddy viscosity closures for the idealized ABL.

### 3 Extension to unstable surface layer stratification

The two limited length scale turbulence closures discussed in Section 2 can be used to model neutral and stable ABLs without the need of a temperature equation and buoyancy forces. However, it is not possible to model the unstable ABL because the turbulence length scale is only limited, not enhanced, i.e.,  $\ell \leq \kappa z$ . In order to model unstable conditions, we need to extend the models such that the turbulence length scale is enhanced in the surface layer,  $\ell > \kappa z$ , which we present in the following sections for each turbulence closure.

### 3.1 Limited mixing-length model

One can generically parameterize the turbulence length scale  $\ell$  as a ‘parallel’ combination of ASL and ABL scales,

$$\frac{1}{\ell} = \frac{1}{\ell_{\text{ASL}}} + \frac{1}{\ell_{\text{ABL}}} \quad (9)$$

Blackadar (1962) chose  $\ell_{\text{ASL}} = \kappa z$  and  $\ell_{\text{ABL}} = \ell_{\text{max}}$  to arrive at Eq. (4). If we choose to set

$$5 \quad \ell_{\text{ASL}} = \frac{\kappa z}{\phi_m} \quad (10)$$

following the turbulence length scale that is a result of Monin-Obukhov Similarity Theory (MOST, Monin and Obukhov (1954))—where

$$\phi_m = (1 - \gamma_1 z/L)^{-1/4} \quad (11)$$

is the dimensionless velocity gradient for unstable conditions, with  $\gamma_1 \approx 16$  as shown by Dyer (1974), and  $L$  is the Obukhov length—then it is possible to extend the limited mixing-length model of Blackadar (1962) to unstable surface layer stratification, as

$$\ell = \frac{\kappa z}{(1 - \gamma_1 z/L)^{-1/4} + \kappa z/\ell_{\text{max}}}. \quad (12)$$

Approaching neutral conditions,  $L^{-1} \rightarrow 0$ , the original length scale model of Blackadar (1962) is obtained. Note that in stable conditions,  $\phi_m = 1 + \beta z/L$ , so the resulting turbulence length can also be rewritten in the Blackadar-type forms form of Eqs. (4) and (9), using an effective maximum turbulence length scale of

$$15 \quad \ell_{\text{ABL,stable}}^{-1} = \ell_{\text{max,eff}}^{-1} \equiv \ell_{\text{max}}^{-1} + \beta/(\kappa L). \quad (13)$$

Thus we can simply use the original length scale model of Blackadar (1962) for stable and neutral conditions; the stable  $\phi_m$  function simply informs the selection of  $\ell_{\text{max,eff}}$ , following Eq. (13).

### 3.2 Limited length scale $k$ - $\varepsilon$ model

20 Sumner and Masson (2012) argued that for stable conditions, the limited length-scale  $k$ - $\varepsilon$  model of Apsley and Castro (1997) overpredicts  $\ell$  in the surface layer compared to MOST, where  $\ell_{\text{max}} = L\kappa/\beta$  and  $\beta \approx 5$ . They proposed a more complicated expression for  $C_{\varepsilon,1}^*$  in the transport equation of  $\varepsilon$  compared to the original model of Apsley and Castro (1997). Sogachev et al. (2012) alternatively prescribed a coefficient in the buoyant term of the  $\varepsilon$  equation, depending on  $\ell/\ell_{\text{max}}$  and being similar to the production-related term that gives results consistent (at least asymptotically) with MOST. We find that the correction of Sumner and Masson (2012) provides a better match of the turbulence length scale within the surface layer compared to MOST with respect to the original  $k$ - $\varepsilon$  model of Apsley and Castro (1997). However, we also find that a larger overshoot of the turbulence length scale around the ABL depth is found when Coriolis is included. Alternatively, one could improve the

surface layer solution of the original model of Apsley and Castro (1997) by simply reducing  $\ell_{\max}$  by roughly 20%. Therefore, we choose to use the model of Apsley and Castro (1997) as our starting point.

In order to account for the increase in turbulence length scale in the surface layer under unstable conditions, we add a buoyancy source term  $\mathcal{B}$  in the  $k$ - $\varepsilon$  transport equations:

$$5 \quad \frac{Dk}{Dt} = \frac{d}{dz} \left( \frac{\nu_T}{\sigma_k} \frac{dk}{dz} \right) + \mathcal{P} - \varepsilon + \mathcal{B} \quad (14)$$

$$\frac{D\varepsilon}{Dt} = \frac{d}{dz} \left( \frac{\nu_T}{\sigma_\varepsilon} \frac{d\varepsilon}{dz} \right) + (C_{\varepsilon,1}^* \mathcal{P} - C_{\varepsilon,2} \varepsilon + C_{\varepsilon,3}^* \mathcal{B}) \frac{\varepsilon}{k}. \quad (15)$$

Here  $\mathcal{B}$  is modeled as

$$\mathcal{B} = -\nu_T \left[ \left( \frac{dU}{dz} \right)^2 + \left( \frac{dV}{dz} \right)^2 \right] \frac{z}{L} = -\nu_T \mathcal{S}^2 \frac{z}{L} \quad (16)$$

following MOST, using the similarity functions of Dyer (1974) as discussed in van der Laan et al. (2017). We use the flow-dependent parameter  $C_{\varepsilon,3}^* \equiv 1 + \alpha_B (C_{\varepsilon,1} - C_{\varepsilon,2})$  of Sogachev et al. (2012), which for unstable conditions includes the prescription

$$\alpha_B = 1 - \left[ 1 + \frac{(C_{\varepsilon,2} - 1)}{(C_{\varepsilon,2} - C_{\varepsilon,1})} \right] \frac{\ell}{\ell_{\max}}, \quad (17)$$

amenable to the free-convection limit:  $\varepsilon/B \rightarrow 1$  for  $P/B \rightarrow 0$ ,  $\varepsilon/B \rightarrow 1$  for  $P/B \rightarrow 0$ . Further,  $\alpha_B \rightarrow 1$  as  $\ell \rightarrow 0$ , matching neutral conditions since  $z/L$  also vanishes then. The prescription (Eq. (17)) results in

$$15 \quad C_{\varepsilon,3}^* = 1 + C_{\varepsilon,1} - C_{\varepsilon,2} + (2C_{\varepsilon,2} - C_{\varepsilon,1} - 1) \frac{\ell}{\ell_{\max}}, \quad (18)$$

which also means that  $C_{\varepsilon,3}^* \rightarrow C_{\varepsilon,2}$  approaching the effective ABL top ( $\ell \rightarrow \ell_{\max}$ ), so that sources and sinks of  $\varepsilon$  balance in Eq. (15); i.e.  $\mathcal{P} - \varepsilon + \mathcal{B}$  all have the same coefficient  $C_{\varepsilon,2}$ .

## 4 Methodology of numerical simulations

The one-dimensional numerical simulations are performed with EllipSys1D (van der Laan and Sørensen, 2017a), which is a simplified one-dimensional version of EllipSys3D, initially developed by Sørensen (1994) and Mikkelsen (2003). EllipSys1D is a finite volume solver for incompressible flow, with collocated storage of flow variables. It is assumed that the vertical velocity is zero and the pressure gradients are constant, which is valid in an idealized ABL, as discussed in Section 2. As a consequence, it is not necessary to solve the pressure correction equation that is normally used to ensure mass conservation.

### 4.1 Ambient turbulence in the limited length-scale $k$ - $\varepsilon$ turbulence model

25 The limited length scale  $k$ - $\varepsilon$  model typically simulates an eddy viscosity that decays to zero for  $z \rightarrow \infty$ , which can lead to numerical instability. While e.g. Koblitz et al. (2015) chose to set upper limits for  $k$  and  $\varepsilon$  to prevent numerical instabilities,

we prefer a more physical method, including ambient source terms  $S_{k,\text{amb}}$  and  $S_{\varepsilon,\text{amb}}$  to the  $k$  and  $\varepsilon$  transport equations, respectively. Following Spalart and Rumsey (2007), we set

$$S_{k,\text{amb}} = \varepsilon_{\text{amb}}, \quad S_{\varepsilon,\text{amb}} = C_{\varepsilon,2} \frac{\varepsilon_{\text{amb}}^2}{k_{\text{amb}}}. \quad (19)$$

When all sources of turbulence are zero ( $\mathcal{P} = B = 0$ ) and the diffusion terms are zero ( $dk/dz = d\varepsilon/dz = 0$ ), then  $k = k_{\text{amb}}$  and  $\varepsilon = \varepsilon_{\text{amb}}$ . To be consistent with the equations solved, we define the ambient turbulence quantities in terms of the driving parameters,  $G$  and  $\ell_{\text{max}}$ :

$$\ell_{\text{amb}} = C_{\text{amb}} \ell_{\text{max}}, \quad k_{\text{amb}} = \frac{3}{2} I_{\text{amb}}^2 G^2, \quad \varepsilon_{\text{amb}} = C_{\mu}^{3/4} \frac{k_{\text{amb}}^{3/2}}{\ell_{\text{amb}}} = C_{\mu}^{3/4} \frac{3}{2} \sqrt{\frac{3}{2}} \frac{I_{\text{amb}}^3}{C_{\text{amb}}} \frac{G^3}{\ell_{\text{max}}}. \quad (20)$$

Here  $I_{\text{amb}}$  is the total turbulence intensity<sup>1</sup> above the (simulated) ABL, and  $C_{\text{amb}}$  is the ratio of the turbulence length scale above the ABL ( $\ell_{\text{amb}}$ ) to maximum turbulence length scale ( $\ell_{\text{max}}$ ). We choose small values for  $I_{\text{amb}} = 10^{-6}$  and  $C_{\text{amb}} = 10^{-6}$ , such that the ambient turbulence does not affect the solution for  $U$  and  $V$ , while the numerical stability is maintained. It should be noted that the overshoot in  $\ell/\ell_{\text{max}}$  that can occur near the ABL depth is still affected by the ambient values. Sogachev et al. (2012) and Koblitz et al. (2015) chose to use a limiter on  $\varepsilon$  to avoid an overshoot in  $\ell$ , but we choose not use it. In general, we prefer to avoid limiters because they can break the Rossby number similarity that is presented in Section 5.

## 4.2 Numerical setup

The flow is driven by a constant pressure gradient using a prescribed constant geostrophic wind speed. The initial wind speed is set to geostrophic wind speed at all heights. During the solving procedure, the ABL depth grows from the ground until convergence is achieved, which occurs when the growth rate of the ABL depth is negligible because a balance between the prescribed pressure gradient, the Coriolis forces and the turbulence stresses is obtained. The flow that we are solving is relatively stiff, and we choose to include the transient terms using a second order three level implicit method with a large time step that is set as  $1/|f_c|$  s. All spatial gradients are discretized by a second order central difference scheme. Convergence is typically achieved after  $10^5$  iterations, which takes about 10 s on a single 2.7 GHz CPU. The domain height is set to  $10^5$  m to assure that the ABL depth is significantly smaller than the domain height for all flow cases considered. The numerical grid represents a line, where the first cell height is set to  $10^{-2}$  m. The cells are stretched for increasing heights using an expansion ratio of about 1.2. The grid consists of 384 cells, which is based on a grid refinement study presented in Section 4.3. A rough-wall-rough-wall boundary conditions is set at the ground, as discussed by Sørensen et al. (2007). For the length scale limited  $k$ - $\varepsilon$  model, this means that we set  $\varepsilon$  at the first cell, use a Neumann condition for  $k$ , and the shear stress at the wall is defined by the neutral surface layer. The first cell is placed on top of the roughness length, which allows us to choose the first cell height independent of the roughness length. This means that we add the roughness length to all relations that include  $z$ , i.e.,  $z + z_0$ . For the limited mixing-length model, we simply set the eddy viscosity from the neutral surface layer at the first cell. Neumann conditions are set for all flow variables at the top boundary.

<sup>1</sup>From the two-equation  $k$ - $\varepsilon$  model (which is isotropic), the total turbulence intensity is calculated by  $I = \sqrt{2/3k}/\sqrt{U^2 + V^2}$ .

The turbulence model constants of the  $k$ - $\varepsilon$  model are set as  $(C_\mu, \sigma_k, \sigma_\varepsilon, C_{\varepsilon,1}, C_{\varepsilon,1}, \kappa) = (0.03, 1.0, 1.3, 1.21, 1.92, 0.4)$ . The chosen  $C_\mu$  value is based on neutral ASL measurements, as discussed by Richards and Hoxey (1993), and  $C_{\varepsilon,1}$  is used to maintain the neutral ASL solution of the  $k$ - $\varepsilon$  model.

### 4.3 Grid refinement study

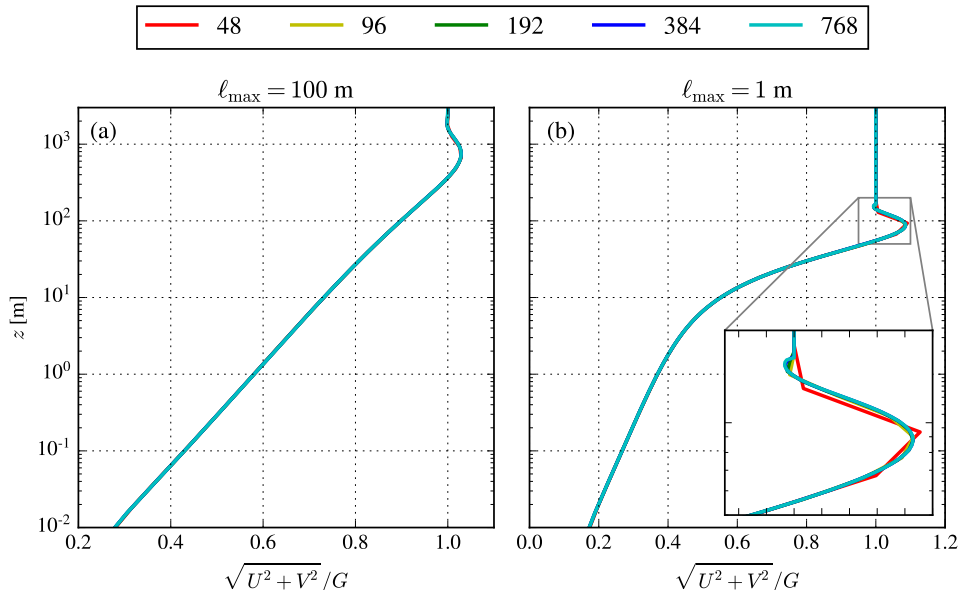


**Figure 2.** Grid refinement study of the one-dimensional RANS simulation using the limited length scale  $k$ - $\varepsilon$  model, for 48, 96, 192, 384 and 768 cells. (a)  $\ell_{\max} = 100$  m. (b)  $\ell_{\max} = 1$  m.

5 A grid refinement study of the numerical setup is performed for the limited length scale  $k$ - $\varepsilon$  model of Apsley and Castro (1997), using 48, 96, 192, 384 and 768 cells. We choose  $f_c = 10^{-4} \text{ s}^{-1}$ ,  $z_0 = 10^{-4} \text{ m}$  and  $G = 10 \text{ ms}^{-1}$  for  $\ell_{\max} = 100$  and  $\ell_{\max} = 1$  m. The results in terms of wind speed of each grid are depicted in Fig. 2 for both values of  $\ell_{\max}$ . For  $\ell_{\max} = 100$  m, the largest difference with respect to the finest grid is 0.5 %, 0.2 %, 0.09 % and 0.03% for 48, 96, 192, 384 cells, respectively, located at the first cell near the wall boundary. When using  $\ell_{\max} = 1$  m, a small ABL depth of 100 m is simulated with a sharp low level jet. In the zoomed plot of Fig. 2b, one can see how the grid size affects the low level jet, where the largest difference with respect to the finest grid is 1 %, 0.2 % and 0.04 % and 0.01 %, for 48, 96, 192, 384 cells, respectively. We find similar results for the limited mixing-length model of Blackadar (1962). In addition, the turbulence model extensions to unstable surface layer stratification typically shows smaller difference between the grids due to the enhanced mixing and the use of a high  $\ell_{\max}$  value that represents a convective ABL. Hence, our choice of using 384 cells is conservative.

## 5 Rossby number similarity in numerical and analytical solutions

The numerical solution of the original limited length scale turbulence closures of Blackadar (1962) and Apsley and Castro (1997) depend on four parameters:  $f_c$  [ $s^{-1}$ ],  $G$  [ $ms^{-1}$ ],  $\ell_{\max}$  [ $m$ ] and  $z_0$ . Blackadar (1962) argued that the maximum turbulence length scale in the ABL should be proportional to the length scale  $G/|f_c|$ . We find that if both  $\ell_{\max}$  [ $m$ ]. Applying the Buckingham  $\pi$  theorem, it is clear that there should exist two dimensionless numbers that define the entire solution, since the four dimensional parameters only have two dimensions ( $[m]$  and  $z_0$  are proportional to  $G/|f_c|$ ), then the ABL profiles only depend on two dimensionless numbers, which can be written as two Rossby numbers with different characteristic length scales. The Rossby number,  $Ro = U/(|f_c|L)$ , [ $s$ ]. This can be shown by writing a non-dimensional momentum equation in complex form (Eq. 2) using the non-dimensional variables  $W' \equiv W/U$ ,  $\nu'_T = \nu_T/(U\mathcal{L})$  and  $z' = z/\mathcal{L}$ , where  $U$  and  $\mathcal{L}$  are characteristic velocity and length scales, respectively:

$$Ro \frac{d}{dz'} \left( \nu'_T \frac{dW'}{dz'} \right) = iW'. \quad (21)$$

Here,  $Ro$  is the Rossby number,  $Ro = U/(|f_c|\mathcal{L})$ , which describes the ratio of the inertial force with respect (advective) tendency to the Coriolis force, where  $U$ . If we apply the original mixing-length model of Blackadar (1962) for  $\nu'_T$  using Eqns (3) and (4), then Eq. (21) can be written as:

$$Ro \frac{d}{dz'} \left( \left[ \frac{\kappa z'}{1 + \kappa z' \mathcal{L}/\ell_{\max}} \right]^2 \left| \frac{dW'}{dz'} \right| \frac{dW'}{dz'} \right) = iW', \quad (22)$$

where  $\mathcal{L}/\ell_{\max}$  is a second dimensionless number. If we choose  $U = G$  and  $L$  are characteristic velocity and length scales, respectively. We define two Rossby numbers based on the geostrophic wind  $G$  as the characteristic velocity scale, with two different  $\mathcal{L} = z_0$ , we may define two Rossby-like numbers, with characteristic length scales  $\ell_{\max}$  and based on  $z_0$  and  $\ell_{\max}$ , respectively:

$$Ro_{\ell 0} \equiv \frac{G}{|f_c| \ell_{\max}} \frac{G}{|f_c| z_0}, \quad Ro_{0\ell} \equiv \frac{G}{|f_c| z_0} \frac{G}{|f_c| \ell_{\max}}. \quad (23)$$

Here, we have obtained  $Ro_{\ell}$  by rewriting the second dimensionless number  $\mathcal{L}/\ell_{\max}$  as the ratio of the two Rossby numbers:  $\mathcal{L}/\ell_{\max} = [U/(|f_c|\ell_{\max})]/[U/(|f_c|\mathcal{L})]$ .  $Ro_0$  is known as the surface Rossby number, first introduced by Lettau (1959);  $Ro_{\ell}$  is analogous to the reciprocal of a dimensionless boundary layer depth (e.g. Arya and Wyngaard, 1975). We define  $\ell_{\max}$  it also resembles a ratio of (inertial) boundary-layer depth to  $z_0$ . Analogously,  $Ro_{\ell}$  is like the ratio of two boundary layer depths,  $f_c/u_{*0}$  and  $z_0$  as:

$$\ell_{\max} = \frac{1}{Ro_{\ell}} \frac{G}{|f_c|}, \quad z_0 = \frac{1}{Ro_0} \frac{G}{|f_c|}$$

Hence  $z_i$  (e.g. Arya and Wyngaard, 1975); here  $\ell_{\max}$  is a proxy for  $z_i$ , acting as a 'lid' for the ABL. Considering Eq. (23), we have reduced the number of dependent parameters from four to two:  $f(f_c, G, \ell_{\max}, z_0) \rightarrow f(Ro_{\ell}, Ro_0) f(f_c, G, \ell_{\max}, z_0) \rightarrow f(Ro_0, Ro_{\ell})$ .

For a fixed surface roughness  $z_0$ , then the ratio of the two Rossby numbers is the only dependent parameter:

$$\ell_{\max} = \frac{\text{Ro}_0}{\text{Ro}_\ell} z_0; \quad (24)$$

i.e., the ratio of simulated ABL depth to  $z_0$  is the lone parameter. Blackadar (1962) found a characteristic maximum ABL turbulence length scale of  $0.00027G/|f_c|$  for the Leipzig wind profile (Lettau, 1950), which equating with  $\ell_{\max}$  corresponds to  $\text{Ro}_\ell \simeq 3700$ .

Figure 3 depicts the Rossby number similarity of our one-dimensional RANS simulations using the original limited length scale turbulence closures of Blackadar (1962), Fig. 3a-c, and Apsley and Castro (1997), Fig. 3d-g. Four combinations of  $\text{Ro}_0$  ( $10^6$  and  $10^9$ ) and  $\text{Ro}_\ell$  ( $10^3$  and  $10^5$ ) are used, each simulated with four combinations of  $G$  (10 and 20  $\text{ms}^{-1}$ ) and  $f_c$  ( $5 \times 10^{-5}$  and  $10^{-4} \text{ s}^{-1}$ ). The roughness length and maximum turbulence length scale follow from Eq. (23) and cover a wide range ~~from~~  $z_0 = 10^{-4} - 0.4 \text{ m}$  and ~~from~~  $\ell_{\max} = 1 - 4 \times 10^2 \text{ m}$  of  $z_0$  from  $10^{-4}$  to 0.4 m, and  $\ell_{\max}$  of 100–400 m. Figure 3 shows that normalized wind speed, wind direction and turbulence quantities for both turbulence closures are only dependent of  $\text{Ro}_0$  and  $\text{Ro}_\ell$ . Both turbulence closures ~~produces~~ produce similar results in terms of wind speed, wind direction and eddy-viscosity. The limited length scale  $k$ - $\varepsilon$  model of Apsley and Castro (1997) also predicts a total turbulence intensity  $I$  (Fig. 3g) and a turbulence length scale  $\ell$  (not shown in Fig. 3), which are only dependent on the two Rossby numbers. In addition, the total turbulence intensity close to the surface only depends on  $\text{Ro}_0$ , while further away, it is mainly influenced by  $\text{Ro}_\ell$  with a weaker dependence on  $\text{Ro}_0$ .

Considering the non-neutral ABL with Coriolis effects but ignoring the strength of capping-inversion (entrainment), in the micrometeorological literature the Kazanski-Monin (1961) parameter  $u_{*0}/(|f_c|L)$  is typically invoked (e.g. Arya, 1975; Zilitinkevich, 1989). This can also be considered like a third Rossby number, which in our context of using  $G$  instead of  $u_{*0}$  is

$$\text{Ro}_{L_-} \equiv \frac{-G}{|f_c|L}; \quad (25)$$

here the subscript ( $L_-$ ) denotes that Eq. (25) is defined for unstable conditions, i.e.  $L \leq 0$ . For the convective boundary layer,  $u_{*0}/(-|f_c|L)$  is generally replaced by the dimensionless inversion height  $-z_i/L$ , because the convective ABL depth does not have a significant dependence on  $u_{*0}/f_c$  (Arya, 1975). However, we note that  $\text{Ro}_{L_-}$  functions as a ‘bottom-up’ parameter in the non-neutral RANS equation set, with the Obukhov length  $L$  in Eq. (16) specified as a surface-layer quantity; in effect  $\text{Ro}_{L_-}$  dictates the relative increase in mixing-length (i.e. in the dimensionless coordinate  $z|f_c|/G$ ). Our length scale limited turbulence closures extended to unstable surface layer stratification, as presented in Section 3, are dependent on  $\text{Ro}_{L_-}$ . This becomes clear when we substitute the mixing-length model extended to unstable surface layer stratification from Eq. (12) in the non-dimensional momentum equation from Eq. (21):

$$\text{Ro} \frac{d}{dz'} \left( \left[ \frac{\kappa z'}{(1 - \gamma_1 z' \mathcal{L}/L)^{-1/4} + \kappa z' \mathcal{L}/\ell_{\max}} \right]^2 \left| \frac{dW'}{dz'} \right| \frac{dW'}{dz'} \right) = iW', \quad (26)$$

where  $\mathcal{L}/L$  is a third non-dimensional number, which can also be written as the ratio of two Rossby numbers:  $\text{Ro}_{L_-}/\text{Ro}_0$ . For  $\text{Ro}_{L_-} = 0$ , the extended models return to the original models. Figure 4 depicts the Rossby number similarity of the extended

$Ro_0, Ro_\ell$	$f_c[s^{-1}], G[ms^{-1}]$	$f_c[s^{-1}], G[ms^{-1}]$	$f_c[s^{-1}], G[ms^{-1}]$	$f_c[s^{-1}], G[ms^{-1}]$
$10^6, 10^3$ :	$5 \times 10^{-5}, 10$	$5 \times 10^{-5}, 20$	$10^{-4}, 10$	$10^{-4}, 20$
$10^6, 10^5$ :	$5 \times 10^{-5}, 10$	$5 \times 10^{-5}, 20$	$10^{-4}, 10$	$10^{-4}, 20$
$10^9, 10^3$ :	$5 \times 10^{-5}, 10$	$5 \times 10^{-5}, 20$	$10^{-4}, 10$	$10^{-4}, 20$
$10^9, 10^5$ :	$5 \times 10^{-5}, 10$	$5 \times 10^{-5}, 20$	$10^{-4}, 10$	$10^{-4}, 20$

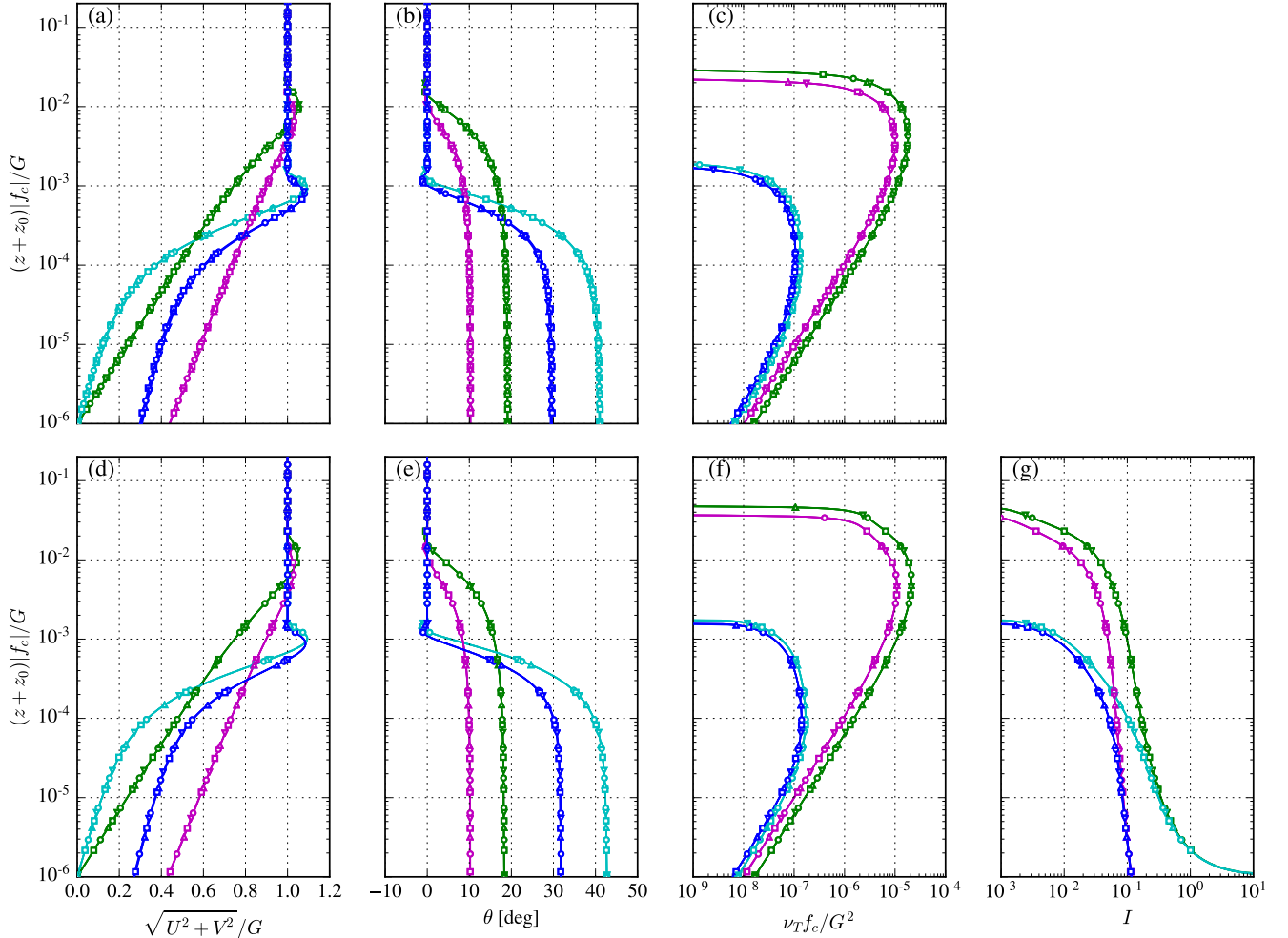


**Figure 3.** Rossby number similarity of the original turbulence closures. **(a-c)** Limited mixing-length model. **(d-g)** Limited length scale  $k$ - $\varepsilon$  model.

turbulence closures using six combinations of the three Rossby numbers, which are each simulated with four combinations of  $G$  and  $f_c$ . We use two values of  $Ro_0$  ( $10^6$  and  $10^9$ ) and three values of  $Ro_{L-}$  ( $0$ ,  $5 \times 10^2$  and  $2 \times 10^3$ ) for  $Ro_\ell = 10^3$ . For these Rossby number combinations,  $Ro_{L-} = 5 \times 10^2$  and  $Ro_{L-} = 2 \times 10^3$  correspond to near-unstable conditions ( $-1/L = 0.00125$ -

0.005 m<sup>-1</sup>) and unstable to very unstable conditions ( $-1/L = 0.005\text{--}0.02\text{ m}^{-1}$ ), respectively. Figure 4 shows the both extended turbulence closures only depend on  $Ro_0$ ,  $Ro_{L_-}$ , for a given  $Ro_\ell$ . Although not shown in Fig. 4, changing  $Ro_\ell$  would not break the Rossby number similarity. Note that it does not make sense to include combinations of non zero values of  $Ro_{L_-}$  that correspond to unstable conditions and large values of  $Ro_\ell$  that corresponds to stable conditions.

5 The extended limited length scale mixing-length model (Fig. 4a-c) is less sensitive to  $Ro_{L_-}$  compared to the extended limited length scale  $k\text{-}\varepsilon$  model (Fig. 4d-g) because of the buoyancy production in the transport equations of  $k$  and  $\varepsilon$ , which is not present in the extended mixing-length model. Both models predict a deeper ABL (larger  $z_i$ ) that is more mixed, for stronger unstable surface layer stratification (increasing  $Ro_{L_-}$ ). The wind veer is also reduced for stronger unstable conditions for the extended  $k\text{-}\varepsilon$  model (Fig. 4e), but it does not always decrease for increasing unstable conditions for the extended mixing-length  
10 model (Fig. 4b).

One could choose to use the friction velocity at the surface,  $u_{*0}$ , as a velocity scale in the Rossby numbers instead of the geostrophic wind speed. However, the friction velocity depends on height  $z$ , and is a result of the model, not an input. In other words, the height at which the friction velocity needs to be extracted to get a collapse is also dependent on the ABL profiles, since the height scales with friction velocity. Hence it is more sensible to use geostrophic wind speed as a velocity scale in the  
15 model-based Rossby number similarity—consistent also with classic Ekman theory (which relates the wind speed in terms of  $G$ ). Nevertheless, it is possible to obtain a Rossby similarity using  $u_{*0}$  as the velocity scale, which is presented in Appendix B.

The Rossby number similarity can be employed to generate a library of ABL profiles for a range of  $Ro_0$ ,  $Ro_\ell$  and  $Ro_{L_-}$ . The library contains all possible model solutions for the range of chosen Rossby numbers and it can be used to determine inflow  
20 profiles for three-dimensional RANS simulations, without the need of running one-dimensional precursor simulations.

The obtained Rossby number similarity can only be achieved for a grid independent numerical setup, as we have shown in Section 4.3. In addition, the ambient source terms should also be scaled by the relevant input parameters ( $G$  and  $\ell_{\max}$ ), as discussed in Section 4.1.

The ABL depth  $z_i$  predicted by the original limited length scale turbulence closures are mainly dependent on the maximum  
25 turbulence length scale  $\ell_{\max}$ . The normalized ABL depth ( $(z_i + z_0)|f_c|/G$ ) is mainly dependent on  $Ro_\ell$ , which is depicted in Fig. 5, where results of the limited length scale  $k\text{-}\varepsilon$  model extended to unstable surface layer stratification are shown for  $3 \times 6 \times 3$  combinations of the three Rossby numbers  $Ro_0$ ,  $Ro_\ell$  and  $Ro_{L_-}$ . We have chosen  $G = 10\text{ ms}^{-1}$  and  $f_c = 10^{-4}\text{ s}^{-1}$ , but the results are independent of  $G$  and  $f_c$  due to the Rossby number similarity. The normalized ABL depth is defined as the height at which the wind direction (relative to the ground) becomes zero for the second time, i.e. above the mean jet  
30 and associated turning as in Ekman theory. For the Ekman solution (Section A1), this definition results in an ABL depth equal to  $z_i = 2\pi\sqrt{2\nu_T/|f_c|}$ . The normalized ABL depth in the RANS model increases for stronger unstable surface layer conditions (larger  $Ro_{L_-}$ ), i.e. for larger values of the surface heat flux. For neutral and stable conditions ( $Ro_{L_-} = 0$ ) and moderate to shallow ABL depths, i.e.  $3 \times 10^3 \leq Ro_\ell \leq 3 \times 10^4$ —corresponding to  $z_i < \sim 2000\text{ m}$  as seen in Fig. 5—we find that  
 $\log_{10}([z_i + z_0]|f_c|/G) \propto a \log_{10}(Ro_\ell) \log_{10}([z_i + z_0]|f_c|/G) \propto -a \log_{10}(Ro_\ell)$ , with  $a = 0.57\text{--}0.62$  for  $Ro_0$  over the range of  
35  $10^9\text{--}10^5$ . Hence for moderate to shallow ABLs the effective depth modeled in neutral and stable conditions is roughly  $z_i \propto$

$Ro_0, Ro_\ell, Ro_{L-}$	$f_c[s^{-1}], G[ms^{-1}]$	$f_c[s^{-1}], G[ms^{-1}]$	$f_c[s^{-1}], G[ms^{-1}]$	$f_c[s^{-1}], G[ms^{-1}]$
$10^6, 10^3, 0:$	$5 \times 10^{-5}, 10$	$5 \times 10^{-5}, 20$	$10^{-4}, 10$	$10^{-4}, 20$
$10^9, 10^3, 0:$	$5 \times 10^{-5}, 10$	$5 \times 10^{-5}, 20$	$10^{-4}, 10$	$10^{-4}, 20$
$10^6, 10^3, 5 \times 10^2:$	$5 \times 10^{-5}, 10$	$5 \times 10^{-5}, 20$	$10^{-4}, 10$	$10^{-4}, 20$
$10^6, 10^3, 2 \times 10^3:$	$5 \times 10^{-5}, 10$	$5 \times 10^{-5}, 20$	$10^{-4}, 10$	$10^{-4}, 20$
$10^9, 10^3, 5 \times 10^2:$	$5 \times 10^{-5}, 10$	$5 \times 10^{-5}, 20$	$10^{-4}, 10$	$10^{-4}, 20$
$10^9, 10^3, 2 \times 10^3:$	$5 \times 10^{-5}, 10$	$5 \times 10^{-5}, 20$	$10^{-4}, 10$	$10^{-4}, 20$

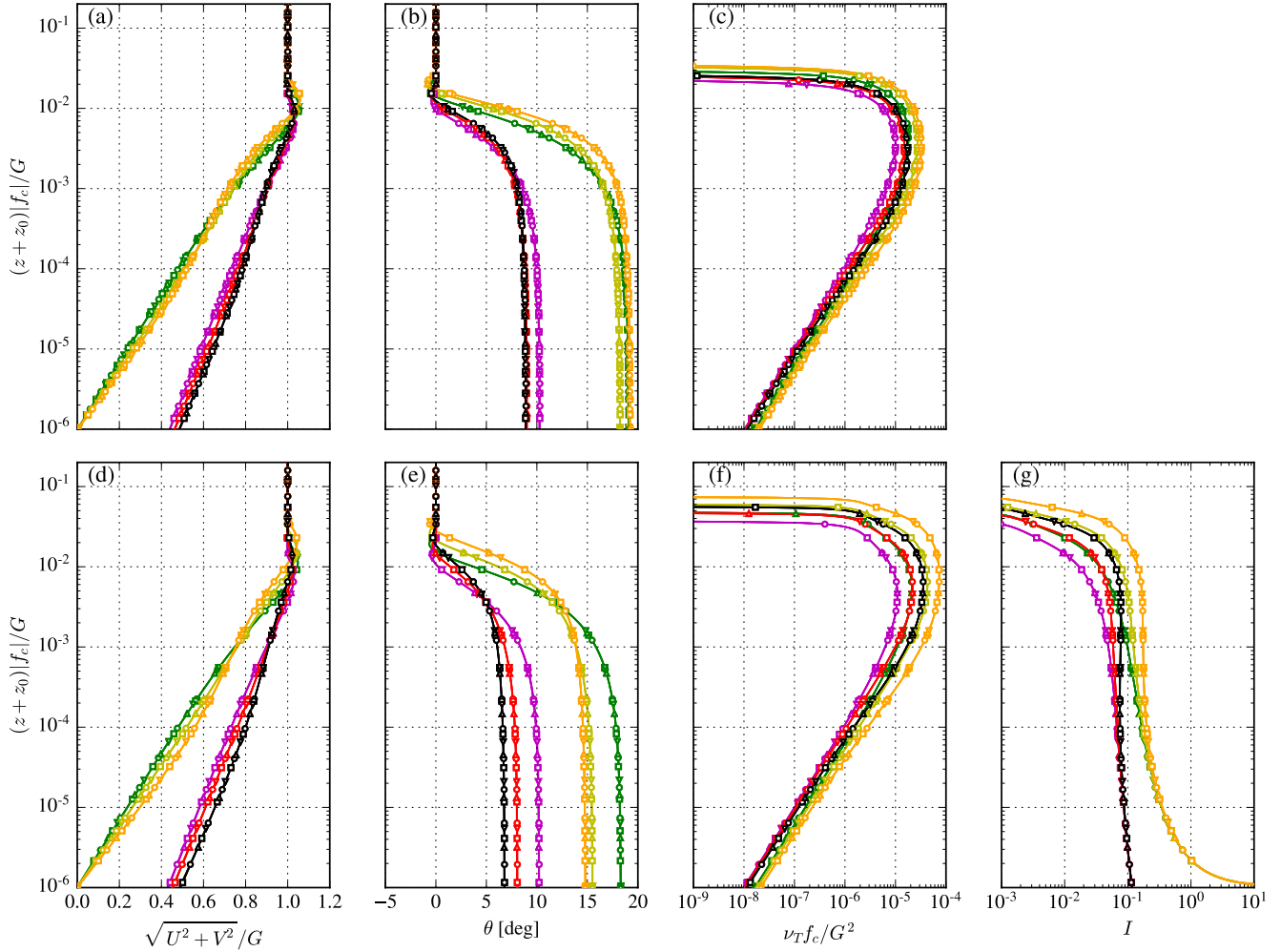


**Figure 4.** Rossby number similarity of the turbulence closures extended to unstable surface layer conditions. **(a-c)** Limited mixing-length model. **(d-g)** Limited length scale  $k-\epsilon$  model.

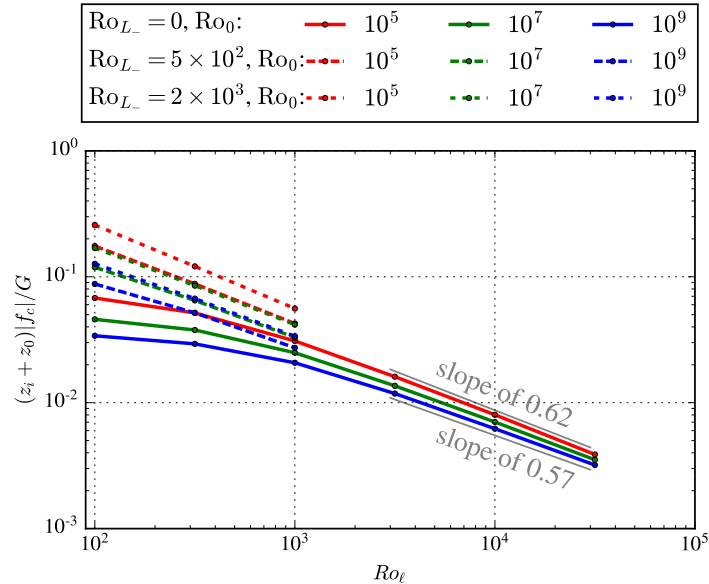


**Figure 5.** Normalized boundary layer depth  $z_i$  predicted by limited length scale  $k$ - $\varepsilon$  model extended to unstable surface layer stratification, as function of the three Rossby numbers.

$\ell_{\max}^a (G/|f_c|)^{1-a}$ , with  $a \approx 0.6$ . As seen by the solid lines in Fig. 5, under neutral conditions and large ABL depths, the  $z_i$  dependence on  $\ell_{\max}$  softens ( $a < 2/3$ ) and deviates from a power law, while for unstable conditions  $a$  is similar to the previously found value of 0.6.

## 6 Validation and model limits

- 5 We employ the Rossby similarity from Section 5 to validate a range of results simulated by the original limited length scale  $k$ - $\varepsilon$  model of Apsley and Castro (1997) including our proposed extension to unstable surface layer stratification. Historical measurements of the geostrophic drag coefficient  $u_{*0}/G$  and the cross isobar angle (the angle between the surface wind direction and the geostrophic wind direction), as summarized by Hess and Garratt (2002), and measured profiles of the ASL and ABL for different atmospheric stabilities from Peña et al. (2010) and Peña et al. (2014), respectively, are used as validation
- 10 metrics. The limited mixing-length model of Blackadar (1962) and its extension are not considered in the comparison with measurements, since we are mainly interested in the  $k$ - $\varepsilon$  model.

### 6.1 Geostrophic drag coefficient

The geostrophic drag law (GDL) is a widely used relation in boundary-layer meteorology and wind resource assessment (after Troen and Petersen, 1989), which connects the surface layer properties as  $z_0$  and  $u_{*0}$  with the driving forces on top of the ABL

proportional to  $|f_c|G$ :

$$G = \frac{u_{*0}}{\kappa} \sqrt{\left[ \ln \left( \frac{u_{*0}}{|f_c|z_0} \right) - A \right]^2 + B^2}, \quad (27)$$

where  $A$  and  $B$  are empirical constants. The GDL can be derived from Eq. (1), where the Reynolds-stresses do not need to be modelled explicitly (as in e.g. Zilitinkevich, 1989), and can be expressed as an implicit relation for the geostrophic drag coefficient  $u_{*0}/G$  and  $Ro_0$ :

$$\frac{u_{*0}}{G} = \frac{\kappa}{\sqrt{\left[ \ln(Ro_0) + \ln \left( \frac{u_{*0}}{G} \right) - A \right]^2 + B^2}}. \quad (28)$$

Figure 6 is a reproduction from Hess and Garratt (2002), where the geostrophic drag coefficient is depicted as function of surface Rossby number  $Ro_0$ . The black markers are measurements summarized by Hess and Garratt (2002), where the dots are near-neutral and near-barotropic conditions, the triangles and squares reflect less idealized atmospheric conditions and the open circles are measurements with a relative high uncertainty. Results of the limited length scale  $k$ - $\varepsilon$  model including the extension to unstable surface layer stratification are shown as colored markers, where the colors represent a range of  $Ro_\ell$ . For the two smallest values of  $Ro_\ell$ , two additional results are plotted for  $Ro_{L-} = 5 \times 10^2$  and  $Ro_{L-} = 2 \times 10^3$ , representing unstable ( $-1/L = 0.005 \text{ m}^{-1}$ ) and very unstable conditions ( $-1/L = 0.02 \text{ m}^{-1}$ ) for the chosen values of  $G = 10 \text{ ms}^{-1}$  and  $f_c = 10^{-4} \text{ s}^{-1}$ . The colored lines are fitted  $A$  and  $B$  constants from the GDL as defined in Eq. (28). The analytic solutions from Ekman (1905) and Ellison (1956), as summarized in Appendix A, are shown as black and gray lines, respectively. For  $Ro_{L-} = 0$ , the geostrophic drag coefficient predicted by the limited length scale  $k$ - $\varepsilon$  model is bounded by the analytic solutions. For  $Ro_\ell \rightarrow 0$ , the geostrophic drag coefficient of Ellison (1956) is approximated. For increasing  $Ro_\ell$  or decreasing ABL depths, the  $\{u_{*0}/G, \log(Ro_0)\}$  relationship becomes more linear. In addition, for  $Ro_\ell = 3.7 \times 10^3$ , as used by Blackadar (1962), and  $Ro_{L-} = 0$ , most of the near-neutral and near-barotropic measurements are captured quite well. Hess and Garratt (2002) used the measurements of the geostrophic drag coefficient to validate a number of models, which often have only one result for each  $Ro_0$ . The geostrophic drag coefficients predicted by the limited length scale  $k$ - $\varepsilon$  model can cover all measurements by varying  $Ro_\ell$ . In addition, the extension to unstable surface layer conditions, can also explain the trend of the more uncertain measurements (black dots). Since  $Ro_\ell$  and  $Ro_{L-}$  influence the ABL depth, as previously shown in Fig. 5, the model suggests that the measurements were conducted for a range of ABL depths that could reflect a range of atmospheric stabilities, although the geostrophic wind shear can play a role here as shown by Floors et al. (2015).

The fitted  $A$  and  $B$  parameters in Fig. 6 are dependent on  $Ro_\ell$  and  $Ro_{L-}$ , which both influence the ABL depth. Typically This is not a surprising result, since many authors showed that  $A$  and  $B$  are dependent on atmospheric stability (see, e.g., Arya, 1975; Zilitinkevich, 1989). For moderate roughness lengths over land, the measured values tabulated by Hess and Garratt (2002) generally fall between the blue and yellow lines for neutral conditions, which are consistent with the typically used values in wind energy are, i.e.,  $A = 1.8$  and  $B = 4.5$  (e.g. Troen and Petersen, 1989), which quite closely matches the blue line ( $Ro_\ell = 10^4, A = 1.82, B = 8.90$ ). Assuming  $\ell_{\max}$  is a measure of the ABL depth, then in the actual atmosphere over land we have  $Ro_0/Ro_\ell \sim 10^3$ - $10^5$ , while over sea the ratio is roughly  $10^6$ - $10^7$ . Thus one can see that the typical wind energy values of  $A$  and  $B$  are a compromise for

Analytic solution:	— Ekman (1905)	— Ellison (1956)			
$k$ - $\varepsilon$ , $Ro_{L_-} = 0$ , $Ro_\ell$ :	• $10^2$	• $10^3$	• $3.7 \times 10^3$	• $10^4$	• $5 \times 10^4$
Fitted ( $A, B$ ):	— 1.93, 3.15	— 2.00, 4.42	— 2.03, 6.47	— 1.82, 8.90	— -0.04, 14.8
$k$ - $\varepsilon$ , $Ro_{L_-} = 5 \times 10^2$ , $Ro_\ell$ :	■ $10^2$	■ $10^3$			
Fitted ( $A, B$ ):	- - 2.94, 0.00	- - 2.49, 2.88			
$k$ - $\varepsilon$ , $Ro_{L_-} = 2 \times 10^3$ , $Ro_\ell$ :	▲ $10^2$	▲ $10^3$			
Fitted ( $A, B$ ):	- - 4.67, 0.00	- - 3.54, 1.97			

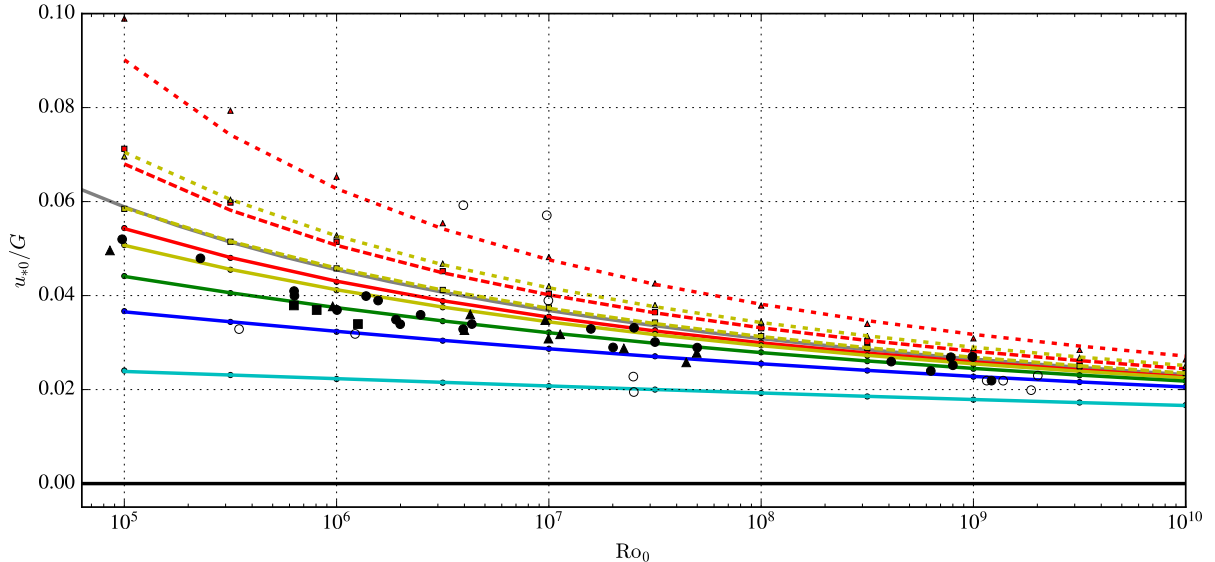


**Figure 6.** Reproduced from Hess and Garratt (2002). Geostrophic drag coefficient simulated by the limited length scale  $k$ - $\varepsilon$  model extended to unstable surface layer stratification, taken at a normalized height of  $(z+z_0)|f_c|/G = 5 \times 10^{-5}$  (i.e., in the surface layer), for different  $Ro_0$ ,  $Ro_\ell$  and  $Ro_{L_-}$ . Black markers represent measurements from Hess and Garratt (2002).  $Ro_\ell = 3.7 \times 10^3$  represents  $\ell_{\max}$  from Blackadar (1962). Analytic results of Ekman (1905) and Ellison (1956) are summarized in Appendix A

applicability over both land and sea. The real-world limits mean that the result for  $Ro_\ell = 10^2$  (red line) can extend only from  $Ro_0 \sim 10^5$ – $10^7$ , while the overseas regime (large  $Ro_0$ ) tends to involve a smaller range of  $Ro_\ell$ . We remind that the GDL from Eq. (27) limits how large  $B$  can be; generally  $u_{*0}/G < \kappa/B$ , so values of  $B$  greater than those shown are not physical. The model results in Fig. 6 do not violate this limit.

## 5 6.2 Cross isobar angle

Figure 7 is a reproduction of Hess and Garratt (2002), where the angle between surface wind direction and the geostrophic wind direction is plotted as function of the surface Rossby number. This angle is known as the cross isobar angle,  $\theta_0$ . The black markers, analytic solutions and model results follow the same definition as used in Fig. 6, where additional black diamond

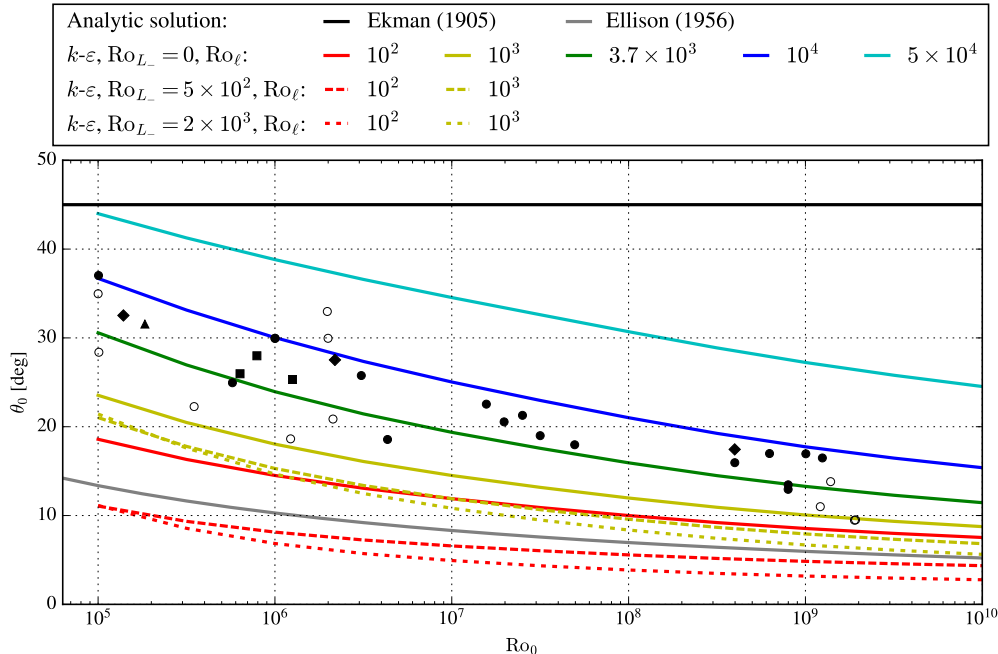


**Figure 7.** Reproduced from Hess and Garratt (2002). Cross isobar angle simulated by the limited length scale  $k$ - $\varepsilon$  model extended to unstable surface layer stratification, taken at a normalized height of  $(z + z_0)|f_c|/G = 5 \times 10^{-5}$  for different  $Ro_0$ ,  $Ro_\ell$  and  $Ro_{L-}$ . Black markers represent measurements from Hess and Garratt (2002).  $Ro_\ell = 3.7$  represents  $\ell_{\max}$  from Blackadar (1962). Analytic results of Ekman (1905) and Ellison (1956) are summarized in Appendix A.

markers are added that correspond to climatological measurements, as discussed by Hess and Garratt (2002). For  $Ro_{L-} = 0$ , the model results of the cross isobar angle are bounded by the analytic solutions, as also found for the geostrophic drag coefficient in Fig. 6. All measurements summarized by Hess and Garratt (2002) can be simulated by the limited length scale  $k$ - $\varepsilon$  model by varying the ABL depth using  $Ro_\ell$ . Most of the measurements are well predicted for  $Ro_{L-} = 0$  and  $Ro_\ell = 10^3$ – $10^4$ , which is the range used by Blackadar (1962) ( $Ro_\ell = 3.7 \times 10^3$ ). For  $Ro_{L-} \neq 0$ , smaller values of the cross isobar angle can be simulated compared the analytic solution of Ellison (1956) due to the enhanced rate of mixing. The model cannot predict larger values of the cross isobar angle compared to the analytic solution of Ekman (1905) ( $45^\circ$ ).

### 6.3 Atmospheric surface layer profiles

Peña et al. (2014) used measurements of the wind speed components from 10 to 160 m, from The National Test Station for Wind Turbines at Høvsøre, a coastal site in Denmark, characterized as flat grassland. The Coriolis parameter for the test location is  $1.21 \times 10^{-4} \text{ s}^{-1}$ . The measurements were taken from sonic anemometers over one year, and a wind direction sector was selected to avoid the influence of the coastline and wind turbine wakes. Peña et al. (2014) also calculated a ‘mixing’

(turbulence) length scale  $\hat{\ell}$  using a local friction velocity  $u_*$  and the wind speed gradient:

$$\hat{\ell} = \frac{u_*}{dU/dz}. \quad (29)$$

Seven cases were defined based on the atmospheric stability, and these are listed in Table 2 in terms of the Obukhov length, roughness length and friction velocity. In order to apply the limited length scale  $k$ - $\varepsilon$ , we need to set the geostrophic wind

Case	Data			Model		
	$1/L$ [m <sup>-1</sup> ]	$z_0$ [m]	$u_{*0}$ [ms <sup>-1</sup> ]	Fitted $G$ [ms <sup>-1</sup> ]	Fitted $\ell_{\max}$ [m]	$u_{*0}$ [ms <sup>-1</sup> ]
Very unstable (vu)	$-1.35 \times 10^{-2}$	$1.3 \times 10^{-2}$	0.35	8.00 (7.50)	$10^3$ ( $5.39 \times 10^2$ )	0.30 (0.34)
Unstable (u)	$-7.04 \times 10^{-3}$	$1.2 \times 10^{-2}$	0.41	10.1 (9.56)	$10^3$ ( $5.54 \times 10^2$ )	0.37 (0.40)
Near unstable (nu)	$-3.18 \times 10^{-3}$	$1.2 \times 10^{-2}$	0.40	10.3 (10.0)	$10^3$ ( $2.00 \times 10^2$ )	0.37 (0.39)
Neutral (n)	$1.87 \times 10^{-4}$	$1.3 \times 10^{-2}$	0.39	11.0	$4.01 \times 10^1$	0.37
Near stable (ns)	$3.14 \times 10^{-3}$	$1.2 \times 10^{-2}$	0.36	11.3	$1.72 \times 10^1$	0.35
Stable (s)	$9.61 \times 10^{-3}$	$0.8 \times 10^{-2}$	0.26	9.96	$6.49 \times 10^0$	0.27
Very stable (vs)	$3.57 \times 10^{-2}$	$0.2 \times 10^{-2}$	0.16	8.62	$3.35 \times 10^0$	0.20

**Table 2.** ASL validation cases. Fitted  $G$ , fitted  $\ell_{\max}$  and modeled  $u_{*0}$  in parenthesis represent values for extended model.

5 speed and the maximum turbulence length scale, which are both unknown. We choose to use  $G$  and  $\ell_{\max}$  as free parameters, which we fit for a reference wind speed and a turbulence length scale, at a reference height of 60 m. The wind speed gradient is obtained from a central difference scheme taking the wind speed at 40, 60 and 80 m. The fitted parameters are obtained by running the numerical simulations with a gradients based optimizer, and the results are listed in Table 2. The maximum  $\ell_{\max}$  is set to  $10^3$  m, which corresponds to an ABL depth on the order of 5 km, as depicted in Fig. 5. The unstable cases are also  
10 simulated with the extended limited length scale  $k$ - $\varepsilon$  model using the measured  $L$ , and re-fitted  $G$  and  $\ell_{\max}$ , which are listed in Table 2 as values in parenthesis.

Fig. 8 depicts the wind speed and turbulence length scale of the measurements and numerical simulations using the original and extended limited length scale  $k$ - $\varepsilon$  models. The turbulence length scale from the numerical simulation is calculated by Eq. (29), instead of the usual definition  $\ell = C_\mu^{3/4} k^{3/2} / \varepsilon$ . The original limited length scale  $k$ - $\varepsilon$  model of Apsley and Castro  
15 (1997) can capture the wind speed and turbulence length scale for the stable and neutral cases. Note that for the very stable case, the shear is under estimated ~~by the model~~ and the model predicts an ABL depth of about 100 m, which results in a spike in  $\hat{\ell}$ , since  $dU/dz$  is zero around the ABL depth. As expected, the original limited length scale  $k$ - $\varepsilon$  model cannot predict a lower shear and a larger turbulence length scale compared to neutral atmospheric conditions (where  $dU/dz = u_*/\ell$  and  $\ell = \kappa z$ ), and the optimizer used to fit  $G$  and  $\ell_{\max}$  sets  $\ell_{\max}$  to our chosen maximum value of  $10^3$  m. Note that therefore the  
20 lines corresponding to unstable conditions of the original  $k$ - $\varepsilon$  model largely overlap in Fig. 8. Higher values of  $\ell_{\max}$  would not improve the results. The limited length scale  $k$ - $\varepsilon$  model extended to unstable surface layer stratification is able to predict turbulence length scales larger than  $\ell = \kappa z$ , and shows improved results for both the shear and the turbulence length scale.

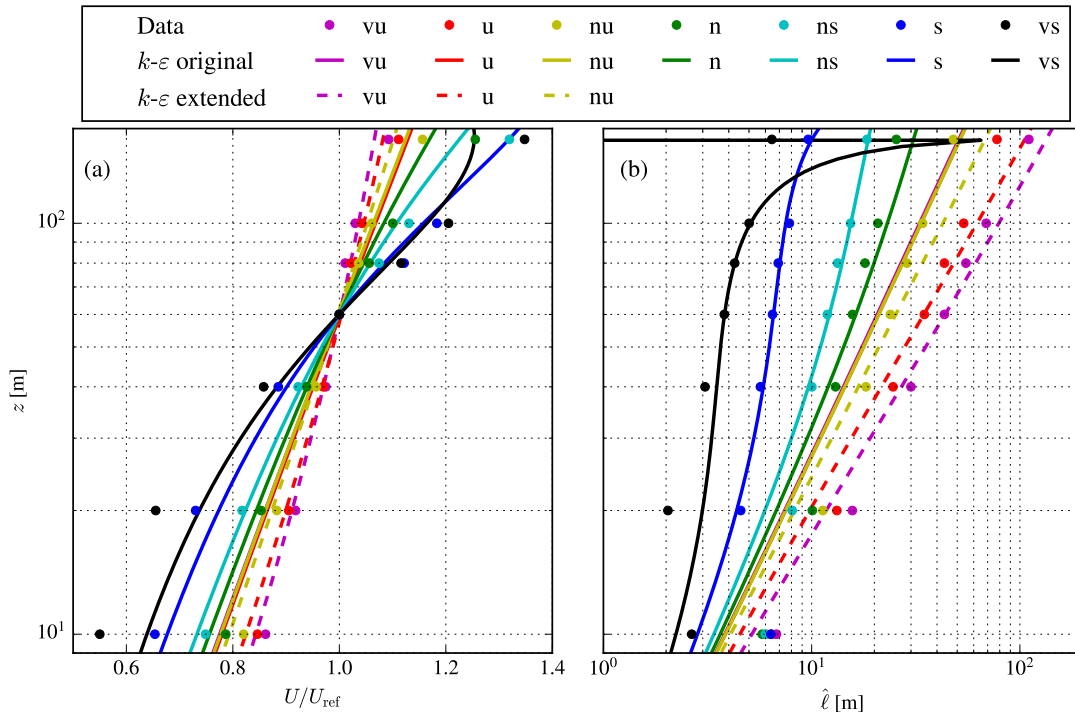


**Figure 8.** ASL measurements of Peña et al. (2010) compared to simulation results of the original limited length scale  $k-\epsilon$  model of Apsley and Castro (1997). **(a)** Wind speed. **(b)** Turbulence length scale from Eq. (29). Unstable cases are also simulated with our extension to unstable surface layer stratification with  $L$  from Table 2.

Table 2 also shows the measured and simulated friction velocity at a height of 10 m. The simulated friction velocity is calculated as  $u_* = (\overline{u'w'^2} + \overline{v'w'^2})^{1/4}$ . For the unstable cases, it clear that the extended model predicts friction velocities that are closer to the measurements compared to the original limited length scale  $k-\epsilon$  model due to the enhanced mixing.

It should be noted that the validation presented in Fig. 8 could be considered as best possible simulation-to-measurement comparison because we have allowed ourselves to tune both  $G$  and  $\ell_{max}$ . When  $G$  is provided by the measurements, it is more difficult to obtain a good match, as shown in Section 6.4.

#### 6.4 Atmospheric boundary layer profiles

Peña et al. (2014) performed lidar measurements of the horizontal wind speed components from 10 to 1200 m at the same test site as discussed in Section 6.3. Ten cases were selected by Peña et al. (2014) that differ in geostrophic forcing and atmospheric stability. The cases were selected to challenge the validation of numerical models. Since our numerical setup can only handle a constant geostrophic wind speed, we select the barotropic cases from Peña et al. (2014): Cases 4, 5 and 9, and the corresponding values of the Obukhov length, geostrophic wind, roughness length, friction velocity,  $Ro_0$  and  $Ro_{L-}$  are listed in Table 3. For convenience, we keep the case names as introduced by Peña et al. (2014). Cases 4 and 5 represent a stable and a neutral ABL

with high forcing, respectively, where  $Ro_0 = 10^7$ . Case 9 is characterized by a low forcing and very unstable stratification, where  $Ro_0 = 2.8 \times 10^6$ .

Case	Description	$1/L$ [m <sup>-1</sup> ]	$G$ [ms <sup>-1</sup> ]	$z_0$ [m]	$u_{*0}$ [ms <sup>-1</sup> ]	$Ro_0$ [-]	$Ro_{L-}$ [-]
4	Stable, strongly forced	$4.5 \times 10^{-3}$	20.5	$1.6 \times 10^{-2}$	0.45	$1.0 \times 10^7$	-
5	Neutral	$-5 \times 10^{-4}$	19.5	$1.6 \times 10^{-2}$	0.70	$1.0 \times 10^7$	-
9	Very unstable, weak forcing	$-4.0 \times 10^{-2}$	5.02	$1.6 \times 10^{-2}$	0.26	$2.8 \times 10^6$	$1.7 \times 10^3$

**Table 3.** ABL validation cases based on Peña et al. (2014).

In Case 6 from Peña et al. (2014) it is observed that the lidar measurements do not approach the geostrophic wind speed at large heights above the surface. This is because the geostrophic wind speed in Peña et al. (2014) is derived from outputs of the Weather Research and Forecasting (WRF) model over a large area, potentially leading to a bias. Therefore, we use a slightly different approach to estimate the geostrophic wind; because the wind speed above the ABL is nearly always in geostrophic balance we can just assume the wind speed measured by the wind lidar above the boundary layer depth to be equal to the geostrophic wind speed, thereby avoiding possible prediction errors in wind speed from the WRF model. Instead, only the ABL depth is estimated from the WRF model outputs. The ABL depth is available as a diagnostic variable predicted by the YSU ABL scheme (Hong et al., 2006) in WRF. To be sure that the lidar wind speed is close to the geostrophic wind speed, we always estimate it from the level that is higher than the modelled ABL depth during all 30-min means, which constitute the three cases.

Since  $G$  is known, we can use the Rossby similarity for the model validation. We could try to find an  $\ell_{\max}$  to get the best comparison with the measurements, but we find that it is difficult to define a good metric. For example, we could try to find an  $\ell_{\max}$  that results in the ABL depth from the measurement cases; however, the ABL depth was not directly measured and only estimated from a model. Instead of finding a single  $\ell_{\max}$  value, we choose to simulate a range of  $\ell_{\max}$  values.

Figure 9 depicts the measured wind speed and wind direction, for each validation case. Since Cases 4 and 5 have the same  $G$  (within 5%) and thus same surface Rossby number  $Ro_0 \simeq 10^7$ , we can plot them together because the normalized model results are the same for both cases. The error bars represent the standard error of the mean. The original limited length scale  $k-\varepsilon$  model of Apsley and Castro (1997) is employed with a range of  $Ro_\ell$ . The unstable ABL case (Case 9) is also simulated with the model extension to unstable surface layer stratification using  $Ro_{L-}$  from Table 3 and the two smallest values of  $Ro_\ell$ . Case 4 has a strong wind shear and a wind veer that leads to a cross isobar angle of  $50^\circ$ . The limited length scale  $k-\varepsilon$  model can predict a maximum cross isobar angle of  $45^\circ$  for extremely shallow ABL depths, as shown in Section 6.2. Hence, the measured ABL from Case 4 is not a possible numerical solution. The measured ABL from Case 5 can be predicted by the original limited length scale  $k-\varepsilon$  model, while this is not the case for the wind speed close to the ground of Case 9 due to the strong unstable stratification. When the limited length scale  $k-\varepsilon$  model including the extension for unstable surface layer conditions is employed, the prediction of the wind speed near the ground is improved, although it is difficult to both get a correct wind

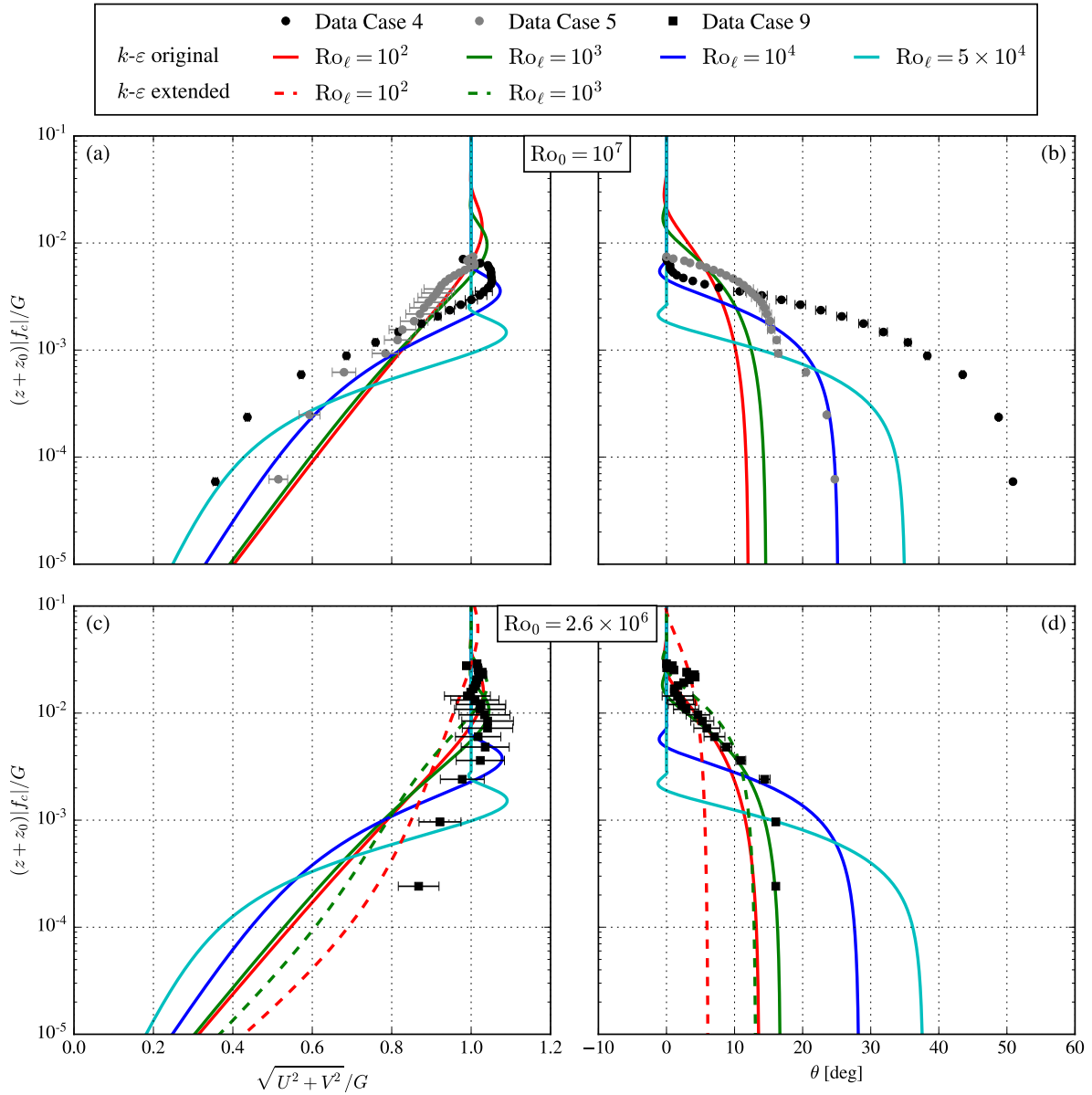


**Figure 9.** ABL measurements from Peña et al. (2014) compared to simulation results of the original limited length scale  $k$ - $\varepsilon$  model of Apsley and Castro (1997), for a range of  $Ro_\ell$ . (a, c) Wind speed. (b, d) Wind direction. Unstable Case 9 is also simulated with our extension to unstable surface layer stratification with  $Ro_{L_-}$  (or  $L$ ) from Table 3.

speed and wind direction. It should be noted that the extended model only improves the wind speed near ground at 10 m. From the measurements during Case 9 it was observed that the WRF-modeled ABL depth grew from 300 m to nearly 1200 m, which indicates that the conditions were largely transient; such non-stationary conditions are difficult for a RANS model. More

unstable cases are necessary to further validate the extended model, including measurements of turbulence quantities such as the (total) turbulence intensity. It is possible to use validation cases based on turbulence-resolving methods, such as large eddy simulation, in future work.

## 7 Conclusions

5 The idealized ABL was simulated with a one-dimensional RANS solver, using two different turbulence closures: a limited mixing-length model, and a limited length scale  $k$ - $\varepsilon$  model. While these models require four input parameters, we have shown that the simulated ABL profiles collapse to a dependence upon two Rossby numbers, which ~~correspond to~~ are defined by the roughness length and the maximum turbulence length scale, respectively. The Rossby number based on the maximum turbulence length scale is a new dimensionless number and is related to the ABL depth. The model-based Rossby number  
10 similarity obtained herein is valid for both turbulence models. We have employed the Rossby number similarity to compare the range of model solutions with historical measurements of relevant associated meteorological quantities, such as the geostrophic drag coefficient and cross-isobar angle. The measured variation in these measurements can be explained by dependence upon the new Rossby number. In addition, we have shown how two classic analytic solutions of the idealized ABL (Ekman, 1905; Ellison, 1956) act as bounds on the results obtainable by the limited length scale  $k$ - $\varepsilon$  model.

15 The limited length scale turbulence closures can represent the effects of stable and neutral stratification, but cannot model unstable conditions. We have proposed simple extensions to overcome this issue, without adding a temperature equation (van der Laan et al., 2017). The extended models require an additional input, the Obukhov length, which can ~~also be written as~~ be used to define a third Rossby number. We have shown that the extension of the  $k$ - $\varepsilon$  model compares well with measurements of seven ASL profiles, representing a range of atmospheric stabilities, including three unstable cases. The  $k$ - $\varepsilon$  model further offers  
20 turbulence intensity, whose profile is also found to collapse according to the developed similarity theories. A model validation of the ~~full~~ ABL for a stable, a neutral and an unstable case is performed, with less success for the non-neutral cases. In the very stable case, the measured wind veer of 50° was larger than the maximum wind veer of 45° that the  $k$ - $\varepsilon$  model can simulate. In addition, the very unstable case was characterized by non-stationary conditions, which are difficult to capture with a RANS model. More validation cases based on the convective ABL are necessary to quantify the performance of the turbulence model  
25 extension to unstable conditions beyond the surface layer.

The application of the one-dimensional RANS simulations to generate inflow profiles for three-dimensional RANS simulations are not performed here and it should be investigated in future work. In addition, the effects of length scale limitation and neglecting the buoyancy force in the momentum equation need to be quantified for three-dimensional RANS simulations of complex terrain and wind farms.

30 *Code and data availability.* The numerical results are generated with proprietary software, although the data presented can be made available by contacting the corresponding author.

*Author contributions.* MPVDL has performed the simulations, obtained the model-based Rossby number similarity for the  $k$ - $\varepsilon$  model, produced all figures and drafted the article. MPVDL and MK proposed the extension to unstable conditions. MK added connections and relations to meteorological theory, and interpretations. AP proposed the Rossby number similarity of the mixing-length model. AP and RF contributed to the model validation. All authors contributed to the methodology and finalization of the paper.

5 *Competing interests.* The authors declare that they have no conflict of interest.

## References

- Apsley, D. D. and Castro, I. P.: A limited-length-scale  $k$ - $\epsilon$  model for the neutral and stably-stratified atmospheric boundary layer, *Boundary-Layer Meteorology*, 83, 75–98, <https://doi.org/10.1023/A:1000252210512>, 1997.
- Arya, S. P. S.: Geostrophic drag and heat transfer relations for the atmospheric boundary layer, *Quart. J. Roy. Meteorol. Soc.*, 101, 147–161, 5 1975.
- Arya, S. P. S. and Wyngaard, J. C.: Effect of baroclinicity on wind profiles and the geostrophic drag law for the convective boundary layer, *J. Atmos. Sci.*, 32, 767–778, 1975.
- Blackadar, A. K.: The vertical distribution of wind and turbulent exchange in a neutral atmosphere, *Journal of Geophysical Research*, 67, 3095–3102, 1962.
- 10 Boussinesq, M. J.: *Théorie de l'écoulement tourbillonnant et tumultueux des liquides*, Gauthier-Villars et fils, Paris, France, 1897.
- Constantin, A. and Johnson, R. S.: Atmospheric Ekman Flows with Variable Eddy Viscosity, *Boundary-Layer Meteorology*, 170, 395–414, <https://doi.org/10.1007/s10546-018-0404-0>, 2019.
- Dyer, A. J.: A review of flux-profile relationships, *Boundary-Layer Meteorology*, 7, 363–372, <https://doi.org/https://doi.org/10.1007/BF00240838>, 1974.
- 15 Ekman, V. W.: On the influence of the earth's rotation on ocean-currents, *Arkiv Mat. Astron. Fysik*, 2, 1905.
- Ellison, T. H.: *Atmospheric Turbulence in Surveys of mechanics*, Cambridge University Press, Cambridge, U. K., 1956.
- Floors, R., Peña, A., and Gryning, S.-E.: The effect of baroclinicity on the wind in the planetary boundary layer, *Q. J. R. Meteorol. Soc.*, 141, 619–630, <https://doi.org/10.1002/qj.2386>, <http://doi.wiley.com/10.1002/qj.2386>, 2015.
- Hess, G. D. and Garratt, J. R.: Evaluating Models Of The Neutral, Barotropic Planetary Boundary Layer Using Integral Measures: Part Ii. 20 Modelling Observed Conditions, *Boundary-Layer Meteorology*, 104, 359–369, <https://doi.org/10.1023/A:1016525332683>, 2002.
- Hong, S.-Y., Noh, Y., and Dudhia, J.: A New Vertical Diffusion Package with an Explicit Treatment of Entrainment Processes, *Mon. Weather Rev.*, 134, 2318–2341, <https://doi.org/10.1175/MWR3199.1>, <http://journals.ametsoc.org/doi/abs/10.1175/MWR3199.1>, 2006.
- Kazanskii, A. and Monin, A.: Dynamic interaction between atmosphere and surface of earth, *Akademiya Nauk Sssr Izvestiya Seriya Geofizicheskaya*, 24, 786–788, 1961.
- 25 Koblitz, T., Bechmann, A., Sogachev, A., Sørensen, N., and Réthoré, P.-E.: Computational Fluid Dynamics model of stratified atmospheric boundary-layer flow, *Wind Energy*, 18, 75–89, <https://doi.org/10.1002/we.1684>, 2015.
- Krishna, K.: The planetary-boundary-layer model of Ellison (1956)—A retrospect, *Boundary-Layer Meteorology*, 19, 293–301, <https://doi.org/10.1007/BF00120593>, 1980.
- Landberg, L.: Short-term prediction of local wind conditions, Tech. rep., Risø National Laboratory, Denmark., 1994.
- 30 Lettau, H.: A Re-examination of the “Leipzig Wind Profile” Considering some Relations between Wind and Turbulence in the Frictional Layer, *Tellus*, 2, 125–129, <https://doi.org/10.1111/j.2153-3490.1950.tb00321.x>, 1950.
- Lettau, H. H.: Wind Profile, Surface Stress and Geostrophic Drag Coefficients in the Atmospheric Surface Layer, *Adv. Geophys.*, 6, 241–257, 1959.
- Mikkelsen, R.: Actuator Disc Methods Applied to Wind Turbines, Ph.D. thesis, Technical University of Denmark, Mek dept, Lyngby, 35 Denmark, 2003.
- Monin, A. S. and Obukhov, A. M.: Basic laws of turbulent mixing in the surface layer of the atmosphere, *Tr. Akad. Nauk. SSSR Geophys. Inst.*, 24, 163–187, 1954.

- Peña, A., Gryning, S.-E., and Mann, J.: On the length-scale of the wind profile, *Quarterly Journal of the Royal Meteorological Society*, 136, 2119–2131, <https://doi.org/10.1002/qj.714>, 2010.
- Peña, A., Floors, R., and Gryning, S.-E.: The Høvsøre Tall Wind-Profile Experiment: A Description of Wind Profile Observations in the Atmospheric Boundary Layer, *Boundary-Layer Meteorology*, 150, 69–89, <https://doi.org/10.1007/s10546-013-9856-4>, 2014.
- 5 Richards, P. J. and Hoxey, R. P.: Appropriate boundary conditions for computational wind engineering models using the  $k$ - $\varepsilon$  turbulence model, *Journal of Wind Engineering and Industrial Aerodynamics*, 46,47, 145–153, 1993.
- Sogachev, A., Kelly, M., and Leclerc, M. Y.: Consistent Two-Equation Closure Modelling for Atmospheric Research: Buoyancy and Vegetation Implementations, *Boundary-Layer Meteorology*, 145, 307–327, <https://doi.org/10.1007/s10546-012-9726-5>, 2012.
- Sørensen, N. N.: General purpose flow solver applied to flow over hills, Ph.D. thesis, Risø National Laboratory, Roskilde, Denmark, 1994.
- 10 Sørensen, N. N., Bechmann, A., Johansen, J., Myllerup, L., Botha, P., Vinther, S., and Nielsen, B. S.: Identification of severe wind conditions using a Reynolds Averaged Navier-Stokes solver, *Journal of Physics: Conference series*, 75, 1–13, <https://doi.org/10.1088/1742-6596/75/1/012053>, 2007.
- Spalart, P. and Rumsey, C.: Effective inflow conditions for turbulence models in aerodynamic calculations, *AIAA J.*, 45, 2544–2553, 2007.
- Sumner, J. and Masson, C.: The Apsley and Castro Limited-Length-Scale  $k$ - $\varepsilon$  Model Revisited for Improved Performance in the Atmospheric Surface Layer, *Boundary-Layer Meteorology*, 144, 199–215, <https://doi.org/10.1007/s10546-012-9724-7>, 2012.
- 15 Troen, I. and Petersen, E. L.: European Wind Atlas, Risø National Laboratory, Roskilde, Denmark, 1989.
- van der Laan, M. P. and Sørensen, N. N.: A 1D version of EllipSys, Tech. Rep. DTU Wind Energy E-0141, Technical University of Denmark, 2017a.
- van der Laan, M. P. and Sørensen, N. N.: Why the Coriolis force turns a wind farm wake clockwise in the Northern Hemisphere, *Wind Energy Science*, 2, 285–294, <https://doi.org/10.5194/wes-2-285-2017>, 2017b.
- 20 van der Laan, M. P., Kelly, M. C., and Sørensen, N. N.: A new k-epsilon model consistent with Monin-Obukhov similarity theory, *Wind Energy*, 20, 479–489, <https://doi.org/10.1002/we.2017>, 2017.
- Zilitinkevich, S. S.: Velocity profiles, the resistance law and the dissipation rate of mean flow kinetic energy in a neutrally and stably stratified planetary boundary layer, *Boundary-Layer Meteorology*, 46, 367–387, 1989.

## 25 **Appendix A: Analytic solutions of the idealized ABL**

### **A1 Constant eddy viscosity: Ekman spiral**

The analytic solution of Ekman (1905), known as the Ekman spiral, can be expressed as a function of a single variable, the normalized height  $\xi \equiv z\sqrt{|f_c|/(2\nu_T)}$ . The wind speed  $S = \sqrt{U^2 + V^2}$  and the wind direction  $\theta$  can be written as:

$$S(\xi) = G\sqrt{1 - 2\cos(\xi)\exp(-\xi) + \exp(-2\xi)}, \quad \theta(\xi) = \arctan\left(\frac{\sin(\xi)}{\exp(\xi) - \cos(\xi)}\right). \quad (\text{A1})$$

- 30 The ~~cross isobar angle,  $\theta_0$~~ , cross-isobar angle  $\theta(0)$  is found to be  $45^\circ$ , and the geostrophic drag coefficient is zero (since there is no roughness or  $u_*$  within Ekman theory).

## A2 Linear eddy viscosity: Ellison

The analytic solution of Ellison (1956) for the  $U$  and  $V$  velocity components can be written in terms of the Kelvin functions  $\ker$  and  $\kei$ , as discussed by Krishna (1980):

$$U = cG \ker(x) + U_G, \quad V = cG \kei(x) + V_G \quad (\text{A2})$$

- 5 where  $x$  is a normalized height  $x \equiv 2\sqrt{z|f_c|/(\kappa u_{*0})}$  and  $c$  is a constant. For  $z \rightarrow z_0$  (and assuming  $z_0 \ll u_{*0}/|f_c|$ ), the Kelvin functions can be expanded, and the solution can be written as:

$$U \approx -cG \left[ \frac{1}{2} \ln \left( \frac{z_0 |f_c|}{\kappa u_{*0}} \right) + \gamma_e \right] + U_G = 0, \quad V \approx -cG \frac{\pi}{4} + V_G = 0 \quad (\text{A3})$$

where  $\gamma_e \approx 0.57721$  is the Euler-Mascheroni constant. We can set the geostrophic wind  $G$  through the constant  $c$ :

$$c = - \left( \left[ \frac{1}{2} \ln \left( \frac{z_0 |f_c|}{\kappa u_{*0}} \right) + \gamma_e \right]^2 + \frac{\pi^2}{16} \right)^{-1/2}, \quad U_G = cG \left[ \frac{1}{2} \ln \left( \frac{z_0 |f_c|}{\kappa u_{*0}} \right) + \gamma_e \right], \quad V_G = cG \frac{\pi}{4} \quad (\text{A4})$$

- 10 Note that Krishna (1980) chose  $cG = -2u_{*0}/\kappa$  (so his  $-c$  is five times the geostrophic drag coefficient  $u_{*0}/G$  for  $\kappa = 0.4$ ), which follows from the Neumann condition:

$$\frac{dU}{dz} = \frac{u_{*0}}{\kappa z} = -\frac{cG}{2z} \quad (\text{A5})$$

by taking  ~~$d/dz$  of  $U$  from~~  $dU/dz$  in Eq. (A2) for  $z \rightarrow z_0$ . As a consequence, the geostrophic wind becomes a dependent parameter. We prefer to keep the geostrophic wind as an independent parameter by using  $c$  as defined in Eq. (A4). Then, the

- 15 effective  $u_{*0}$  is calculated as  $u_{*0,\text{eff}} = cG\kappa/2$ .

A GDL can be derived in [the](#) form of Eq. (28) ~~(by~~ using the Neumann conditions of Eq. (A5) and the constant  $c$  from Eq. (A4), where  $A = -\ln(\kappa) + 2\gamma_e \approx 2.07$  and  $B = \pi/2 \approx 1.57$ , as also shown by Krishna (1980). The friction velocity in Eq. (A4) can now be calculated by solving the GDL for  $u_{*0}/G$ . Hence, the analytic solution of Ellison (1956) is only dependent on  $\text{Ro}_0$ .

- 20 The cross isobar angle (angle between the geostrophic wind direction and surface wind direction) can be written as a function of the geostrophic drag coefficient  $u_{*0}/G$  and the Rossby number  $\text{Ro}_0$  using Eq. (A4):

$$\theta_0 = \arctan \left( \frac{V_G}{U_G} \right) = \arctan \left( \frac{\pi/2}{2\gamma_e - \ln(\text{Ro}_0) - \ln(\kappa u_{*0}/G)} \right) \quad (\text{A6})$$

where the GDL can be used to solve for  $u_{*0}/G$ .

## Appendix B: [Rossby number similarity based on the friction velocity](#)

- 25 [In this article, we have shown a Rossby similarity of two limited length scale turbulence closures using the geostrophic wind speed,  \$G\$ , as a velocity scale, instead of the friction velocity near the ground,  \$u\_{0\*}\$ . It is more convenient to use  \$G\$  because it is](#)

a constant and a model input, while  $u_{0*}$  is a model result that depends on height. However, it is possible to obtain a Rossby similarity based on  $u_{0*}$  using the geostrophic drag coefficient  $u_{*0}/G$  from Fig. 6, since we can write:

$$\text{Ro}_\ell^* \equiv \frac{u_{*0}}{|f_c|\ell_{\max}} = \frac{u_{*0}}{G} \text{Ro}_\ell, \quad \text{Ro}_0^* \equiv \frac{u_{*0}}{|f_c|z_0} = \frac{u_{*0}}{G} \text{Ro}_0, \quad \text{Ro}_{L-}^* \equiv \frac{-u_{*0}}{|f_c|L} = \frac{u_{*0}}{G} \text{Ro}_{L-} \quad (\text{B1})$$

Figure 6 can be transformed to an explicit relation of  $u_{*0}/G$  as function of  $\text{Ro}_\ell^*$ ,  $\text{Ro}_0^*$  and  $\text{Ro}_{L-}$ , the result is depicted in Fig. B1 for  $\text{Ro}_{L-}^* = 0$ .

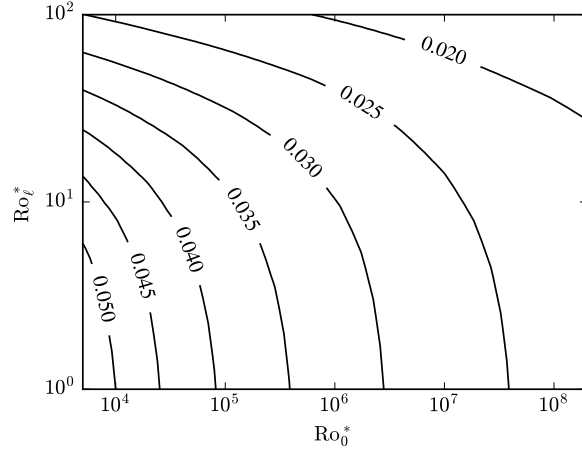


**Figure B1.** Geostrophic drag coefficient simulated by the limited length scale  $k$ - $\varepsilon$  model as function of  $\text{Ro}_\ell^*$  and  $\text{Ro}_0^*$  with  $\text{Ro}_{L-}^* = 0$ .

5

The Rossby similarity based on  $u_{0*}$  is illustrated in Fig. B2 for four combinations of  $\text{Ro}_0^*$  ( $10^5$  and  $10^8$ ) and  $\text{Ro}_\ell^*$  ( $10^2$  and  $10^4$ ), for  $\text{Ro}_{L-} = 0$ , using four combinations of  $u_{*0}$  (0.2 and 0.4  $\text{ms}^{-1}$ ) and  $f_c$  ( $5 \times 10^{-5}$  and  $10^{-4}$   $\text{s}^{-1}$ ). Only results of the limited length scale  $k$ - $\varepsilon$  model are shown for brevity, although the Rossby similarity based on  $u_{0*}$  also applies to the limited mixing-length model and for the unstable extension (where  $\text{Ro}_{L-} \neq 0$ ).

10

It should be noted that  $u_{0*}$  in Fig. 6 was extracted at a normalized height of  $(z+z_0)|f_c|/G = 5 \times 10^{-5}$ , which represents the surface layer. If a perfect Rossby similarity based on  $u_{0*}$  is desired, one would need to extract  $u_{0*}$  at a constant normalized height equal to  $(z+z_0)|f_c|/u_{0*}$ , which requires an iterative process of finding a geostrophic wind speed that results in a RANS simulation with a desired  $u_{0*}$ , at a constant normalized height. This is beyond the scope of the present work.

$Ro_0^*, Ro_\ell^*$	$f_c[s^{-1}], u_{*0}[ms^{-1}]$	$f_c[s^{-1}], u_{*0}[ms^{-1}]$	$f_c[s^{-1}], u_{*0}[ms^{-1}]$	$f_c[s^{-1}], u_{*0}[ms^{-1}]$
$10^5, 10^2$ :	$5 \times 10^{-5}, 0.2$	$5 \times 10^{-5}, 0.4$	$10^{-4}, 0.2$	$10^{-4}, 0.4$
$10^5, 10^4$ :	$5 \times 10^{-5}, 0.2$	$5 \times 10^{-5}, 0.4$	$10^{-4}, 0.2$	$10^{-4}, 0.4$
$10^8, 10^2$ :	$5 \times 10^{-5}, 0.2$	$5 \times 10^{-5}, 0.4$	$10^{-4}, 0.2$	$10^{-4}, 0.4$
$10^8, 10^4$ :	$5 \times 10^{-5}, 0.2$	$5 \times 10^{-5}, 0.4$	$10^{-4}, 0.2$	$10^{-4}, 0.4$

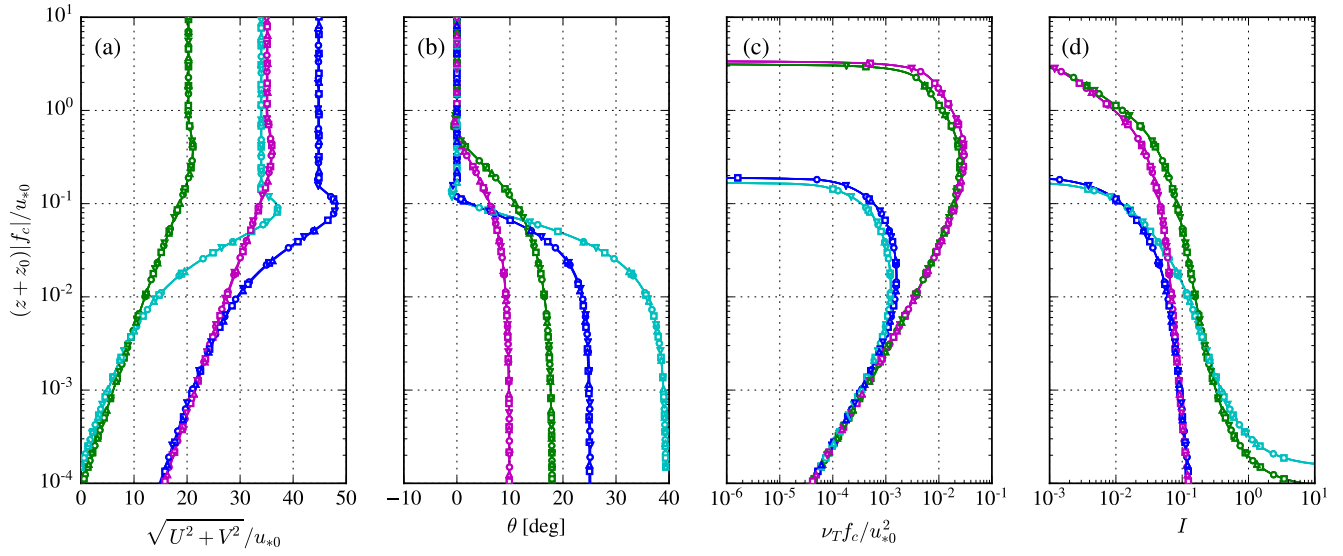


**Figure B2.** Rossby number similarity of the limited length scale  $k$ - $\varepsilon$  model using the friction velocity as the velocity scale, for  $Ro_{L-} = 0$ .